Numerical and experimental study of the behavior of a polyamide during the ECAE process using a 105° die

Houari Habib, Aour Benaoumeur
Laboratory of Applied Biomechanics and Biomaterials, National Polytechnic School of Oran, Algeria
houarihabib@yahoo.fr, http://orcid.org/0009-0007-6626-3996
benaoumeur.aour@enp-oran.dz, http://orcid.org/0000-0003-1300-0790

Ramtani Salah
IUT de Saint-Denis, Département Génie Mécanique et Productique, Laboratoire CB3S, Equipe BEST, France
ramtani@univ-paris13.fr, http://orcid.org/0000-0002-4873-7584

Benalia Faycal
Department of Physics, Higher Normal School of Laghouat Taleb Abderrahmane, Algeria
allfaycal@yahoo.fr, http://orcid.org/0009-0008-9437-8114

Barboura Salma
Laboratoire des Sciences des Procédés et des Matériaux, LSPM - CNRS UPR3407, France
salma.barboura@univ-paris13.fr

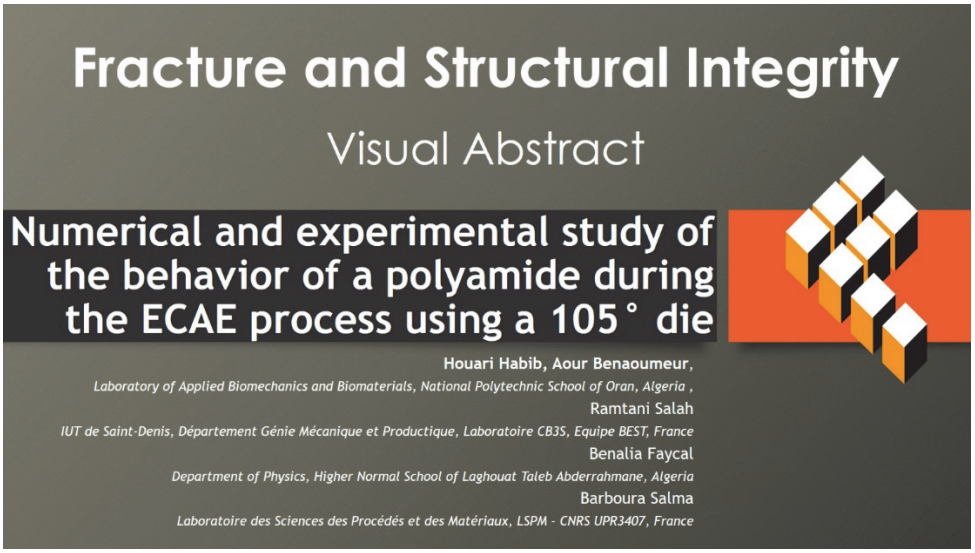

Citation: Houari H., Aour B., Ramtani S., Benalia F, Barboura S., Numerical and experimental Study of the behavior of a polyamide during the ECAE process using a 105° die, Fracture and Structural Integrity, 76 (2026) 238-264.

Received: 16.11.2025
Accepted: 10.01.2026
Published: 13.03.2026
Issue: 04.2026

KEYWORDS. ECAE, Polyamide, Finite element analysis, Equivalent Plastic Strain, Friction.

INTRODUCTION

The equal channel angular extrusion (ECAE) is a processing technique used to induce substantial plastic deformation in materials while preserving the original cross-sectional dimensions of the specimen. The basic principle of the process is illustrated in Fig. 1. Initially developed by Segal et al. [1], this technique has attracted considerable interest as an effective method for enhancing material properties through severe plastic deformation. The process is based on simple shear deformation, achieved by pressing the workpiece through a die with two intersecting channels of equal cross-section. ECAE has proven highly effective in producing ultrafine grain structures in metallic materials [2,3] and in inducing significant molecular orientation in polymeric materials, [4,5,6] both of which result in notable improvements in mechanical properties.

Nowadays, polyamides and other polymers are increasingly replacing metallic materials in various industrial domains. They are widely employed in applications such as mechanical components and electronic devices (e.g., covers, couplers, gears) owing to their relatively low manufacturing cost and versatility [7]. In this context, the equal channel angular extrusion (ECAE) process has been extensively used to enhance the mechanical properties of polymers, and numerous studies have addressed its effects on different polymeric systems. For instance, investigations on linear low-density polyethylene (LLDPE) revealed notable morphological changes induced by ECAE [4]. Sue et al. [8] reported that, in the case of polycarbonate (PC), extrusion must be performed at temperatures slightly below the glass transition to ensure effective processing. Similarly, Li et al. [9] demonstrated that the mechanical properties of PC can be tailored by varying the processing routes and the number of passes. Xia et al. [10] examined the effect of molecular anisotropy on the impact strength of polycarbonate and showed that the improvement in impact resistance is directly related to the changes in molecular orientation induced by the process. Furthermore, Xia et al. [11] identified crystallinity and molecular orientation as key factors influencing the dynamic mechanical properties of ECAE-oriented semi-crystalline polyethylene terephthalate (PET), with improvements observed in both bending and torsional storage moduli.

The influence of different ECAE routes has also been investigated for other polymers. Weon et al. [12] studied polymethyl methacrylate (PMMA) and reported significant variations in tensile, fracture toughness, flexural, and ballistic impact properties depending on the route applied. Recent studies on polypropylene further highlighted the strong dependence of microstructural evolution and mechanical performance on the processing route (e.g., route A versus route C) under back pressure, confirming notable differences in deformation behavior [13].

Beyond experimental work, several reviews have addressed the structural transformations induced by severe plastic deformation in polymers, including semi-crystalline and amorphous polymers, polymer blends and composites, and polymer powders. These works also consider advanced variants of the process, such as equal channel multi-angular extrusion (ECMAE), and their impact on material properties. [14] In parallel, numerical studies have contributed to a better understanding of polymer deformation under ECAE. One notable contribution developed efficient finite element analysis (FEA) models and demonstrated the crucial influence of the constitutive law on predictive accuracy. Comparisons between J2-plasticity, Bergstrom–Boyce, and three-network models revealed significant differences in extrusion load, deformed geometry, and shear strain distribution. The study also emphasized the strong effect of friction on punch force, highlighted the limitations of the plane strain assumption in the presence of billet–die interactions, and showed that sharp die corners can generate a "dead zone" that substantially alters extrusion force and strain distribution [15].

The ECAE process has also been employed to modify the aspect ratio and orientation of clay nanoparticles in nylon-6/clay nanocomposites, as demonstrated by Weon and Sue [16]. Wang et al. [17] provided valuable insights into lamellar formation and relaxation in shear-deformed polyethylene terephthalate (PET) using an in situ time-resolved synchrotron small-angle X-ray scattering (SAXS) technique. More recently, combined numerical and experimental investigations have been carried out to assess the influence of key geometrical and processing parameters on the viscoplastic behavior of polymers during the ECAE process [15,18].

Although Equal Channel Angular Extrusion (ECAE) is a well-established severe plastic deformation technique widely used for metallic materials, its application to polymers remains extremely limited. Existing experimental studies on polymer ECAE are scarce and have been almost exclusively restricted to a small number of channel angles, namely 90°, 120°, and 135°. Moreover, these studies mainly focus on process feasibility and macroscopic deformation, while practical limitations such as extrusion instability at low angles and excessive specimen curvature at higher angles have received little attention. To date, no experimental study has reported the application of ECAE to polyamide materials, despite their extensive industrial use and strong sensitivity to processing-induced deformation. In addition, the evolution of mechanical properties, particularly hardness, under ECAE processing has not yet been investigated for polyamides. In this context, the present work aims to address these gaps by experimentally applying the ECAE process to polyamide for the first time, investigating an intermediate channel angle of 105°, and analyzing the resulting deformation behavior and hardness evolution. This

approach provides new insights into the suitability of ECAE for polyamides and contributes to extending severe plastic deformation concepts to polymeric materials.

In this study, the deformation behavior of polyamide (PA) is investigated using a 105° ECAE die, with the aim of enhancing both the magnitude and homogeneity of plastic strain while minimizing sample warping. To achieve this objective, the paper is structured as follows: Section 2 describes the finite element modeling, while Section 3 compares analytical predictions with FEM results. Section 4 presents the numerical findings on the effects of channel angle, intermediate channel length, and friction on strain distribution, pressing force, and the variation factor V, considering both single-turn and double-turn dies. Section 5 reports the experimental results obtained with 1-ECAE and 2-ECAE configurations, focusing on curvature evolution and hardness. Finally, Section 6 summarizes the main conclusions of the work.

BASIC PRINCIPLE OF THE ECAE PROCESS

The general principle of the ECAE process is illustrated in Fig. 1. The tooling consists of a block incorporating either two (Fig. 1a) or three (Fig. 1b) intersecting channels of identical cross-section. During processing, a specimen inserted into the entrance channel is extruded through the exit channel by means of a punch. When using a 2-ECAE die, the material undergoes two successive shear deformations within a single pass. Compared with the conventional 1-ECAE configuration, this design allows the accumulation of higher plastic strains in fewer passes, thereby improving strain homogeneity and enhancing the efficiency of molecular orientation.

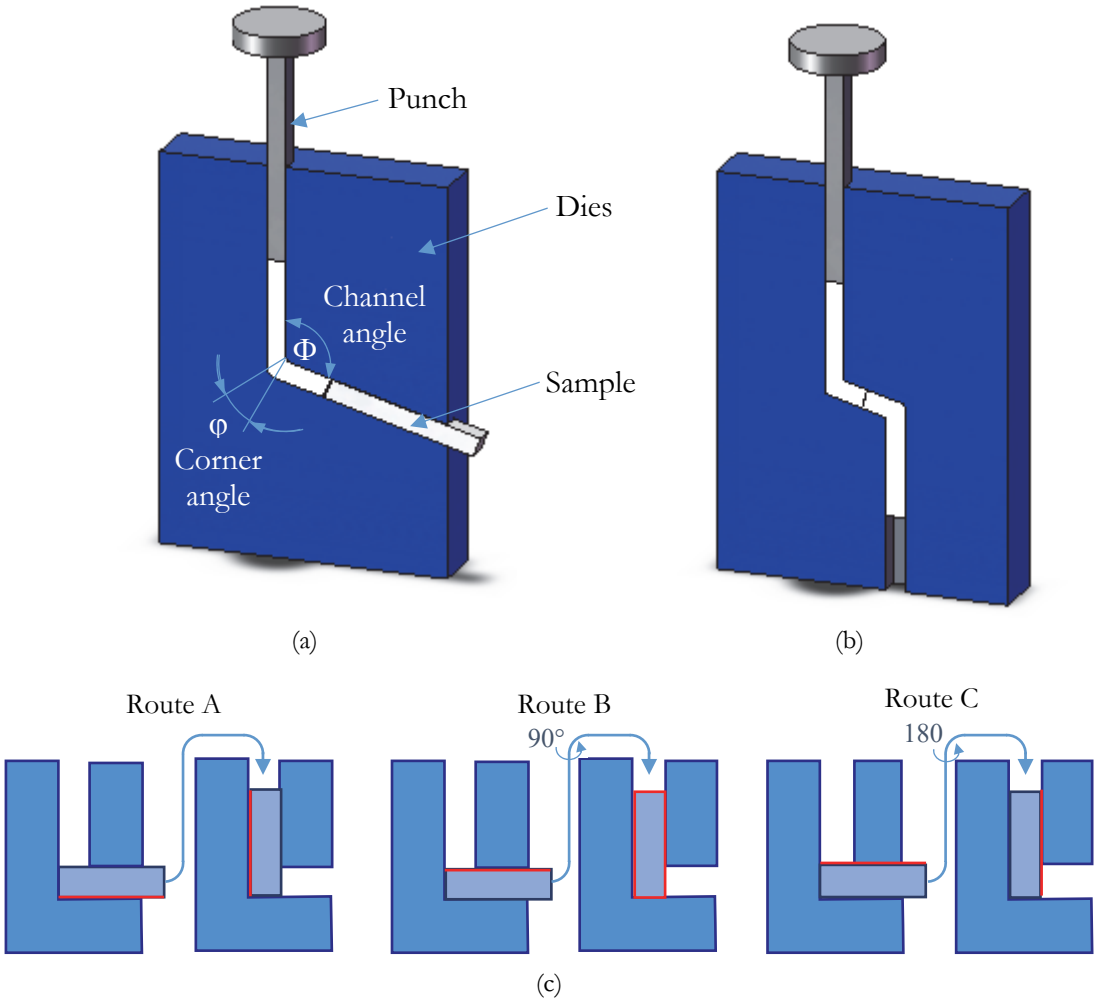

Figure 1: Schematic diagram of equal channel angular extrusion: (a) 1-ECAE, (b) 2-ECAE, and (c) Illustration of Routes A, B, and C.

Theoretically, the Φ angle is arbitrary; the increment of equivalent plastic strain caused by shear as a result of one pass through the channel can be calculated as follows [19]:

$$\dot{\varepsilon}_i = \frac{1}{\sqrt{3}}\left[2\cos\left(\frac{\Phi}{2}+\frac{\varphi}{2}\right)+\varphi\cos ec\left(\frac{\Phi}{2}+\frac{\varphi}{2}\right)\right] \quad (1)$$

where φ is the corner angle.
The total equivalent plastic strain for N cycles is:

$$\varepsilon = N\dot{\varepsilon}_i \quad (2)$$

In the case of the modified ECAE process, known as equal-channel multiple angular extrusion (ECMAE) [20], the billet is extruded through a die consisting of several channels of identical cross-sections intersecting at fixed angles. Under these conditions, the equivalent plastic strain can be expressed as:

$$\varepsilon = \frac{2}{\sqrt{3}}\sum_{i=1}^{n}\cot\frac{\Phi_i}{2} \quad (3)$$

where n is the number of intersection angles of the channels, it should be noted that. ECAE equipment realizes simple shear deformation with varied orientation of shear planes and extrusion with varied deformation intensity.

CONSTITUTIVE MODELING

The mechanical response of polyamide under compression and various strain rates exhibits pronounced time-dependent and rate-sensitive characteristics that cannot be accurately captured by conventional elastic–plastic formulations. To represent this behavior more realistically, the present study employs the Perzyna viscoplastic model [21], combined with a Voce-type nonlinear isotropic hardening law [22]. This constitutive framework provides a physically consistent description of the rate-dependent plastic flow and the saturation of hardening typically observed in polymeric materials. The model is formulated under small strain assumptions and assumes an additive decomposition of the total strain rate into its elastic and plastic components.

$$\dot{\boldsymbol{\varepsilon}} = \dot{\boldsymbol{\varepsilon}}^{e} + \dot{\boldsymbol{\varepsilon}}^{p} \quad (4)$$

where $\dot{\boldsymbol{\varepsilon}}^{e}$ and $\dot{\boldsymbol{\varepsilon}}^{p}$ denote the elastic and plastic strain rates, respectively.
This decomposition assumes that the material response can be separated into a recoverable (elastic) part and a time-dependent irreversible (plastic or viscoplastic) part, as commonly adopted in rate-dependent plasticity formulations. [21,22,23]
The elastic behavior of the polyamide is considered linear and isotropic, following Hooke's law:

$$\dot{\boldsymbol{\sigma}} = \mathbf{C}^{e} : \dot{\boldsymbol{\varepsilon}}^{p} \quad (5)$$

where $\mathbf{C}^{e}$ is the isotropic elasticity tensor defined by Young's modulus E and Poisson's ratio ν. The tensor components can be expressed as:

$$C^{e}_{ijkl} = \lambda\delta_{ij}\delta_{kl} + \mu\left(\delta_{ik}\delta_{jl} + \delta_{il}\delta_{jk}\right) \quad (6)$$

where δ_{ij} is Kronecker delta (δ_{ij} =1 if i=j, otherwise 0), λ and μ are the Lamé parameters.
This formulation ensures that the stress–strain relationship remains consistent with the principles of small deformations and isotropic elasticity.

The elastic parameters E and ν are determined from the initial slope of the experimental stress–strain curves, prior to the onset of plastic deformation. The elastic response provides the foundation upon which the viscoplastic flow rule is subsequently built to describe the rate-dependent inelastic behavior of the polyamide under various strain rates.
The time-dependent viscoplastic behavior of polyamide is modeled using the Perzyna overstress formulation [22,23,24], which assumes that plastic flow is activated once the equivalent stress exceeds a rate-independent yield surface. This approach has been widely used for metallic and polymeric materials exhibiting rate-dependent plasticity [21,25,26]. The total inelastic strain rate is therefore governed by a viscous flow function that depends on the overstress and the strain-rate sensitivity of the material. The onset of plastic flow is governed by a von Mises yield criterion expressed as:

$$f(\boldsymbol{\sigma},\bar{\varepsilon}^{p}) = \sigma_{eq} - \sigma_{y}(\bar{\varepsilon}^{p}) \le 0 \tag{8}$$

where σ_{eq} is the equivalent von Mises stress, and $\mathbf{s}$ denotes the deviatoric part of the Cauchy stress tensor $\boldsymbol{\sigma}$ defined as:

$$\sigma_{eq} = \sqrt{\frac{3}{2}\mathbf{s}:\mathbf{s}} \tag{9}$$

$$\mathbf{s} = \boldsymbol{\sigma} - \frac{1}{3}tr(\boldsymbol{\sigma})\mathbf{I} \tag{10}$$

The isotropic hardening is described by a Voce-type law, which captures the saturation of hardening at large strains [27,28]:

$$\sigma_{y}(\bar{\varepsilon}^{p}) = \sigma_{0} + Q\left[1-\exp(-b\bar{\varepsilon}^{p})\right] \tag{11}$$

where σ_0 is the initial yield stress, Q the saturation stress (maximum hardening amplitude), and b a material parameter controlling the rate of saturation.
This formulation has been widely validated for polymers exhibiting nonlinear hardening [27,29,30]. To account for rate effects, the viscoplastic flow is described using Perzyna's overstress theory [23]. The plastic strain rate is expressed as:

$$\dot{\varepsilon}^{p} = \dot{\gamma}\,\mathbf{n} \tag{12}$$

where $\mathbf{n} = \dfrac{\partial f}{\partial \boldsymbol{\sigma}} = \dfrac{3}{2}\dfrac{\mathbf{s}}{\sigma_{eq}}$ is the flow direction (normal to the yield surface), and $\dot{\gamma}$ is the plastic consistency parameter (or viscoplastic multiplier) defined by the flow function:

$$\dot{\gamma} = \frac{1}{\eta}\left\langle \frac{f(\boldsymbol{\sigma},\bar{\varepsilon}^{p})}{\sigma_{y}(\bar{\varepsilon}^{p})} \right\rangle^{m} \tag{13}$$

where η is a viscosity coefficient controlling the rate dependence, m is the strain-rate sensitivity exponent, and $\langle\cdot\rangle$ denotes the Macaulay brackets, ensuring plastic flow occurs only when f > 0.
This formulation ensures that viscoplastic flow occurs only when the stress state exceeds the instantaneous yield surface, thus maintaining thermodynamic consistency. The equivalent plastic strain rate $\dot{\bar{\varepsilon}}^{p}$ is computed as:

$$\dot{\bar{\varepsilon}}^{p} = \sqrt{\frac{2}{3}\dot{\varepsilon}^{p}:\dot{\varepsilon}^{p}} \tag{14}$$

This set of equations fully defines the elasto-viscoplastic response of the polyamide under multiaxial loading. The model provides a realistic description of strain-rate sensitivity and strain hardening, which are characteristic of semi-crystalline polymers. [29, 30, 31]

It is worth noting that the constitutive model employed in this study is valid under isothermal conditions and assumes a homogeneous, isotropic material response subjected to monotonic severe plastic deformation without damage initiation or evolution. The model is formulated at a macroscopic scale and captures the nonlinear elasto-viscoplastic behavior of the polymer; however, it does not explicitly account for microstructural mechanisms, such as the evolution of crystalline and amorphous phases during deformation. Consequently, the model is expected to provide reliable predictions for the ECAE process under the investigated processing conditions, while its applicability may be limited for non-isothermal loading, cyclic deformation, or deformation regimes involving significant microstructural transformations or damage mechanisms.

Compression test experiment

To identify the six parameters $\{E,\sigma_0,Q,b,\eta,m\}$ of the proposed elasto-viscoplastic model, polyamide specimens were tested under three different true strain rates of 10^{-3}, 10^{-2}, and 10^{-1} s^{-1} at room temperature (25 °C). The uniaxial compression tests were conducted using a Shimadzu universal testing machine equipped with a 50 kN load cell to accurately measure the applied force. The experimental stress–strain data were continuously recorded through the Trapezium acquisition software. The displacement of the upper platen was controlled by adjusting the crosshead speed, which was determined according to the imposed strain rate. Each specimen was compressed up to 55% true strain between two parallel compression plates to ensure uniform deformation.

From the recorded crosshead displacement and the measured applied force F during the test, the nominal stress–strain curves were obtained using the Shimadzu software integrated into the testing system. In order to convert the nominal quantities into true stress and true strain, the material was assumed to be isotropic and incompressible, and the deformation was considered homogeneous. The axial displacement was obtained from the crosshead movement of the testing machine. Knowing the initial specimen height L_0, the true axial strain was calculated from the measured displacement ΔL using the following relation:

$$\varepsilon_{true} = Ln\left(1+\frac{\Delta L}{L_0}\right) \tag{15}$$

The true stress becomes:

$$\sigma_{true} = \sigma_N\left(1+\frac{\Delta L}{L_0}\right) \tag{16}$$

where $\sigma_N = F/S_0$, is the nominal stress and S_0 is the initial section.

Three cylindrical specimens were tested for each deformation rate of 10^{-3}, 10^{-2}, and 10^{-1} s^{-1} to ensure statistical reliability. The specimens had a length of 20 mm and a diameter of 10 mm (L = 2D). Fig. 2 shows the true stress–strain curves obtained from compression tests on polyamide at three different strain rates: $\dot{\varepsilon} = 10^{-1}\,s^{-1}, 10^{-2}\,s^{-1}$ *and* $10^{-3}\,s^{-1}$. A clear strain-rate sensitivity can be observed. At the lowest strain rate ($10^{-3}\,s^{-1}$), the material exhibits a more gradual increase in stress with strain, reflecting greater ductility and enhanced molecular mobility. As the strain rate increases, both the apparent yield stress and flow stress rise significantly, illustrating the typical viscoplastic hardening behavior of semi-crystalline polymers. This rate-dependent strengthening is attributed to the restricted motion of crystalline lamellae and the limited molecular rearrangements within the amorphous regions at higher loading rates. Consequently, the polyamide displays a stiffer mechanical response and higher resistance under rapid deformation. At larger strains, the curves tend to converge, indicating the onset of hardening saturation, which is consistent with nonlinear isotropic hardening laws such as the Voce model or rate-dependent formulations like the Perzyna viscoplastic model.

Parameters identification

The constitutive model is defined by a set of material parameters identified from experimental stress–strain curves obtained at different strain rates, namely $\{E,\sigma_0,Q,b,\eta,m\}$. Parameter identification is performed using uniaxial compression tests

conducted at strain rates of 10^{-3}, 10^{-2}, and 10^{-1} s^{-1}. The optimization procedure aims to minimize the root mean square (RMS) error between the experimental and simulated stress–strain curves. This identification strategy yields a consistent set of parameters capable of accurately reproducing both the rate-dependent yielding and the saturation of strain hardening, in agreement with recent studies [29, 30].

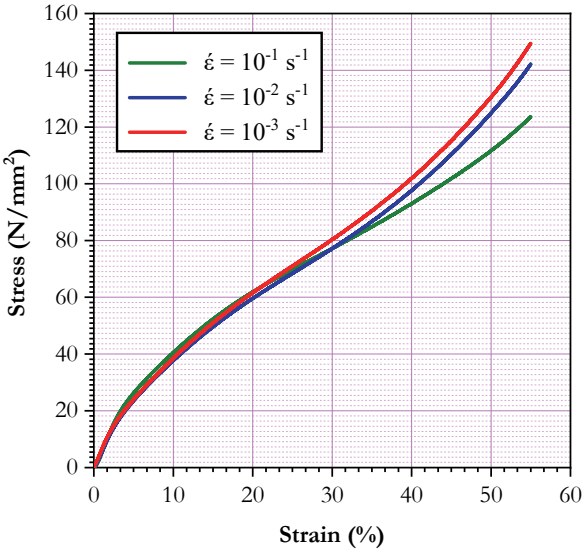

Figure 2: Stress-strain curves of PA 66 at different strain rates $\dot{\varepsilon} = 10^{-1}\,s^{-1}, 10^{-2}\,s^{-1}$ *and* $10^{-3}\,s^{-1}$.

The identified parameters are summarized in Tab. 1, and Fig. 3 shows a good agreement between the experimental data and the numerical simulations. The number of significant digits used in the reported parameters has been adjusted to reflect the experimental uncertainties and the accuracy of the parameter identification procedure. A simple sensitivity analysis was carried out by varying the main material parameters by ±5%. The results indicate that the numerical predictions remain stable within this range, confirming the robustness of the model.

Parameter	Symbole	Identified value
Initial yield stress	σ_0	12 MPa
Hardening amplitude	Q	125 MPa
Hardening rate	b	8
Viscosity parameter	η	38 MPa
Rate sensitivity exponent	n	3.6
Reference strain rate	$\dot{\varepsilon}_0$	$9.4 \times 10^{-2}\ s^{-1}$
Young's modulus	E	2300 MPa

Table 1: Material parameters of the elastic-viscoplastic model for PA 66 at different strain rates.

At room temperature, the strain-rate dependence observed in Fig. 2 remains relatively limited. However, a consistent trend can still be identified over the investigated range of deformation rates, which is sufficient for the calibration of the constitutive model parameters. The calibrated model accurately reproduces the experimental stress–strain responses within the considered deformation domain, demonstrating its robustness and predictive capability under the studied conditions. It should be noted that the present calibration is focused on deformation rates relevant to the ECAE process investigated in this work. A more pronounced strain-rate sensitivity is expected at higher deformation rates and/or different temperature levels, and a more extensive experimental–numerical validation under such conditions is planned as part of future work.

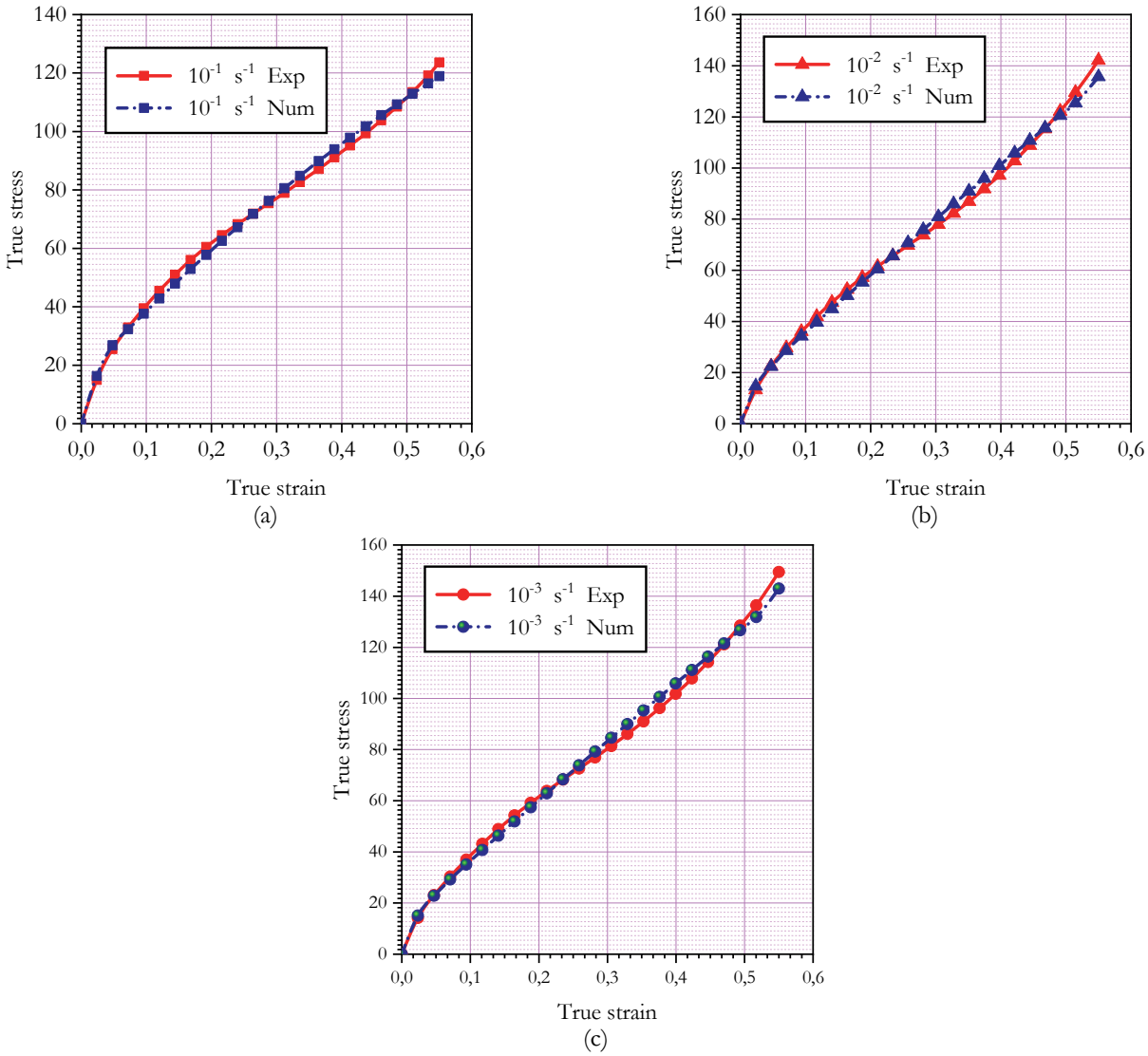

Figure 3: Stress-strain curves of the studied polyamide for different strain rates: (a) 10^{-1} s^{-1}, (b) 10^{-2} s^{-1} and (c) 10^{-3} s^{-1}.

FINITE ELEMENT MODELING

The simulations were carried out using the finite element code MSC.Marc under plane-strain conditions. The sample dimensions were set to 10 mm (width) × 10 mm (thickness) × 100 mm (length). For the die geometry, a channel angle of $\Phi_1 = \Phi_2 = \Phi = 105°$ was considered (corresponding to a 105° die), while the two outer corner angles were varied. The inner corners were modeled with a radius of r = 1 mm [32].

The selection of the channel angle is a critical parameter in the ECAE process, as it directly governs the imposed strain and the material flow behavior. Previous experimental studies on polymer ECAE have mainly focused on channel angles of 90°, 120°, and 135°. For polymers, and particularly for polyamide, severe experimental limitations have been reported for 90° dies, including material blockage at the channel corner and unstable extrusion conditions, which were also observed during preliminary trials in the present work. On the other hand, for channel angles greater than or equal to 120°, extrusion is feasible; however, the curvature of the extruded specimens remains relatively high, limiting deformation efficiency and dimensional stability.

Based on these observations, an intermediate channel angle of 105° was selected in this study as a compromise between process feasibility and effective deformation. This angle facilitates material flow while simultaneously contributing to curvature reduction of the extruded specimens. The present work, therefore, focuses on the experimental and numerical investigation of polyamide processed by ECAE at this intermediate channel angle.

In the modeling, both the die and the ram were assumed to behave as rigid bodies. A displacement of 100 mm was applied to the ram in the extrusion direction. Initially, the friction coefficient between the sample and the die channels was assumed to be zero, corresponding to frictionless contact conditions for the simulations. The finite element calculations were performed under the plane strain assumption. The sample was discretized using four-node isoparametric plane strain elements with reduced integration. A total of 4000 elements was used to mesh the sample, providing a satisfactory compromise between computational efficiency and solution accuracy. The selected mesh density was sufficiently refined to accurately capture the localized deformation occurring during the ECAE process. Based on theoretical [l3] and experimental [33] analyses, the material behavior of the sample was modeled as elasto-viscoplastic. To evaluate the plastic strain distribution, the selected cross-section was taken 20 mm below the first and the second inner corners (see Fig. 4).

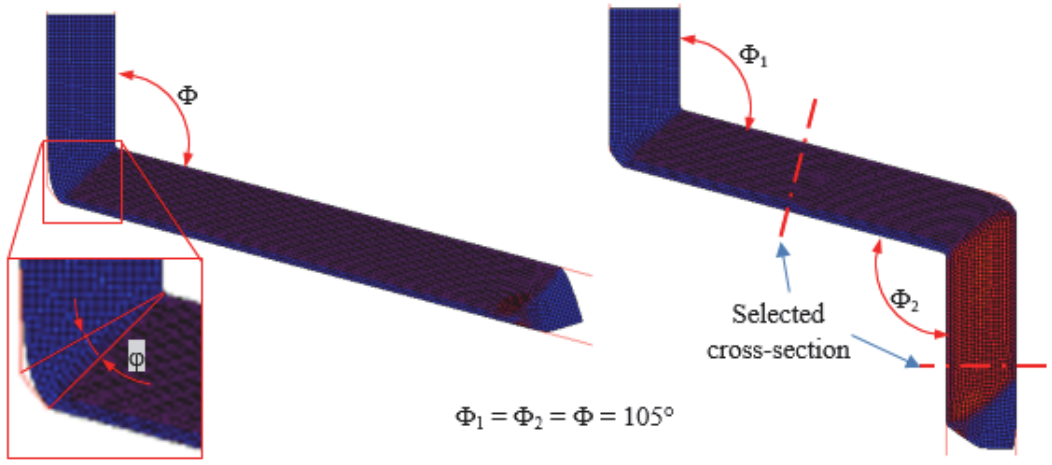

(a) (b)

Figure 4: Illustration of the finite element meshes of the samples for (a) the 105° 1-ECAE die and (b) the 105° 2-ECAE die.

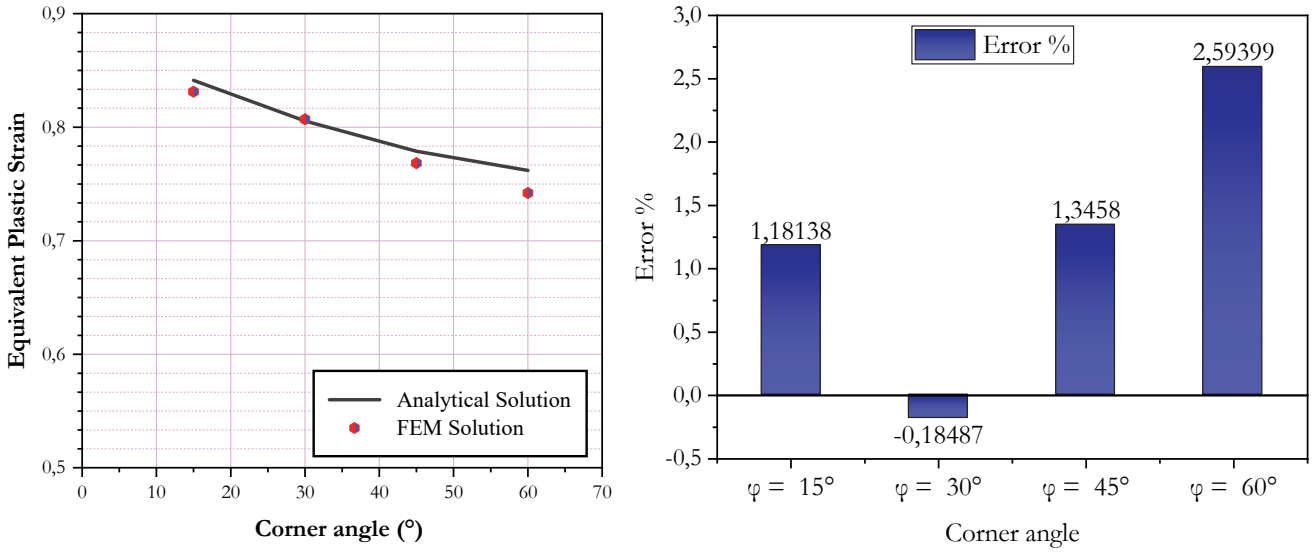

(a) (b)

Figure 5: (a) Comparison between FEM and analytical solutions of the equivalent plastic strain for different corner angles (φ) in the case of a 105° die, (b) The maximum relative error between the analytical and FEM solutions.

CONFRONTATION BETWEEN ANALYTICAL AND FEM RESULTS

To compare the analytical solution given by Eqn. (1) with the FEM results for different corner angles (φ), a perfectly plastic material behavior was assumed at this stage. This assumption neglects hardening and viscous effects, thereby isolating the influence of geometrical factors. The equivalent plastic strain values at the midsection of the workpiece were plotted as a function of the channel angle (Φ = 105°). The results, presented in Fig. 5(a), show that the solid line

corresponds to Eqn. (1), while the data points represent the FEM predictions. It can be seen that a good agreement has been found between the two approaches, as the maximum relative error does not exceed 2.6%, which occurs for a corner angle of φ = 60° (see Fig. 5(b)).
The slight discrepancies between the analytical and numerical results can be attributed to the simplifying assumptions of the analytical formulation, whereas FEM accounts for more realistic stress–strain distributions and boundary conditions. Overall, the close correlation between both approaches demonstrates the reliability of the analytical model for estimating the strain generated during the equal channel angular extrusion (ECAE) process.
Moreover, the results show that increasing the corner angle leads to a progressive decrease in equivalent plastic strain, indicating that sharper die angles induce greater shear deformation in the material.

RESULTS AND DISCUSSION

Case of a 105° 1-ECAE Die - Evolution of the Plastic Strain and the Variation Factor

In the ECAE process, ensuring homogeneous plastic strain distribution within the bulk material during successive passes is crucial. This section aims to identify the optimal conditions that enhance strain homogeneity by examining the influence of the corner angle (φ) and the length (L) of the second channel in the two-elbow die.
The simulations were performed for the case of the 105° die (1-ECAE) following the conditions stated in section 3, and the results are illustrated in Fig. 6. The equivalent plastic strain distribution appears relatively uniform and homogeneous. At a low shear angle (φ = 15°), the deformation remains fairly uniform and constrained, indicating weak strain localization. When the angle increases to φ = 30°, distinct deformation bands begin to emerge, reflecting stronger shear effects. At φ = 45°, these bands become more pronounced, revealing intensified plastic flow and higher strain concentration within the material. Finally, at φ = 60°, the deformation is highly localized, with sharp shear zones dominating the microstructure, highlighting the strong influence of larger shear angles in promoting localized plastic instabilities.

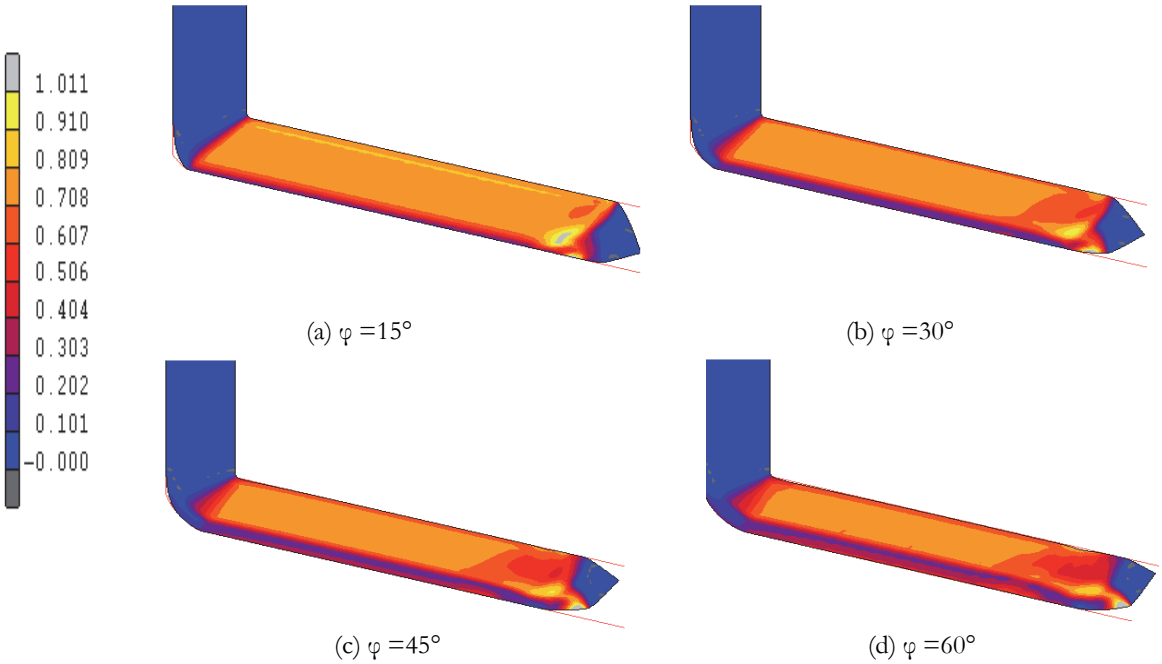

Figure 6: Equivalent plastic strain contours in polyamide for a 105° 1-ECAE die at different corner angles (φ = 15°, 30°, 45°, 60°).

To provide further detail, Fig. 7 presents the evolution of the equivalent plastic strain along the selected cross-section of the sample for different corner angles φ. The results show that the lowest equivalent plastic strain occurs at φ = 60°, whereas the highest strain level is reached at φ = 15°. In all cases, strain is concentrated near the die corner, where intense shear deformation develops. The strain magnitude increases as the corner angle decreases, indicating that sharper die angles promote more pronounced plastic deformation. Nevertheless, the 105° die offers a balance between strain concentration and uniformity, as the deformation is distributed over a wider region compared with sharper angles. This confirms that die

geometry plays a critical role in strain distribution during ECAE, thereby directly affecting the efficiency of microstructural refinement.

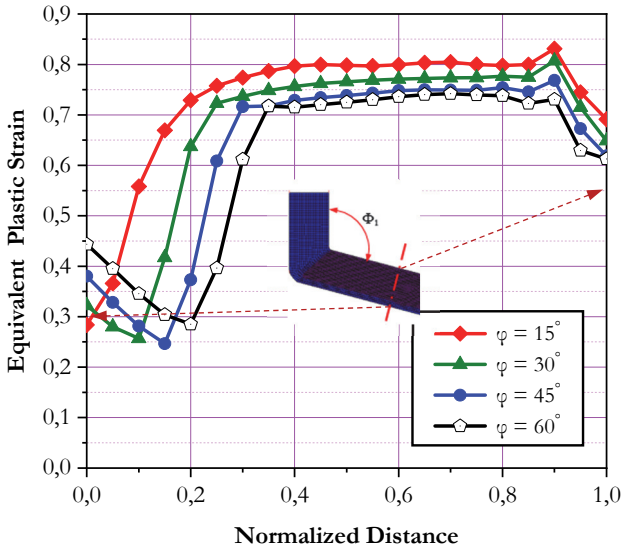

Figure 7: Equivalent plastic strain distribution for various corner angles in a 105° 1-ECAE die. The "normalized distance" corresponds to the distance along the sample thickness, normalized by the total thickness of the sample.

It is interesting to note that the degree of homogeneity of the strain distribution can be assessed through a variation factor V, which is a key parameter for quantifying strain uniformity. Indeed, a higher value of V corresponds to greater heterogeneity of deformation. This factor is given by the following expression[34,35].

$$V = \frac{1}{\dot{\varepsilon}_{ave}} \sqrt{\frac{1}{n} \sum_{i=1}^{n} \left(\dot{\varepsilon}_i - \dot{\varepsilon}_{ave} \right)} \times 100\% \tag{17}$$

where $\dot{\varepsilon}_{ave}$ is the average of the equivalent plastic strain values computed on n integration points, and $\dot{\varepsilon}_i$ is the equivalent plastic strain value of a given integration point along the sample width.

Tab. 2 summarizes the numerical results of the maximum and average values of the equivalent plastic strain, together with the corresponding variation factor, for different corner angles (φ) in the case of the 105° die. These indicators provide complementary insights: while the maximum and average strains reflect the overall deformation intensity, the variation factor highlights the degree of strain heterogeneity within the sample. Such a comparison is essential to assess the influence of die geometry on both the magnitude and uniformity of plastic deformation, thereby allowing a more comprehensive evaluation of the process efficiency. It can be observed that the variation factor decreases as the corner angle φ decreases. Moreover, the average equivalent plastic strain ranges from 0.609 (at φ = 60° with V=28.9%) to 0.723 (at φ = 15° with V=19.8%) in the investigated case. Based on the variation factor criterion, it can be concluded that the best homogeneity of the plastic strain distribution is achieved when the corner angle is φ = 15°.

Conner Angle φ=(°)	Maximum strain ε_{max}	Average strain ε_{ave}	Minimum strain ε_{min}	Variation factor V (%)
15°	0.83	0.723	0.284	19.8
30°	0.807	0.666	0.257	26.3
45°	0.768	0.626	0.247	28.2
60°	0.742	0.609	0.285	28.9

Table 2: Evolution of the equivalent plastic strain and the variation factor in terms of φ in the case of 105° 1-ECAE die.

Evolution of the Pressing Force

Fig. 8 presents the numerical results of the pressing force required for extrusion of polyamide (PA) using a 105° 1-ECAE die. It can be observed that, at the onset of extrusion, the pressing force increases progressively until reaching its maximum value of 6.3998 kN for φ = 15°, and 5.8626 kN for φ = 30°; 5.5388 kN for φ = 45°, and 5.3353 kN for φ = 60°. It should be noted that after the sample exits the first channel junction, the pressing force stabilizes and remains nearly constant until the specimen is fully extruded.

Furthermore, a dimpled trend is observed in the force–plateau region of Fig. 8. Since friction was neglected in the present numerical model, this behavior cannot be associated with a stick–slip mechanism. Instead, it is attributed to the intrinsic non-linear response and intermittent viscoplastic flow of the material under severe shear deformation. Similar oscillatory trends have been reported in the literature for equal-channel angular extrusion processes, notably in the work of Zaïri et al. [5].

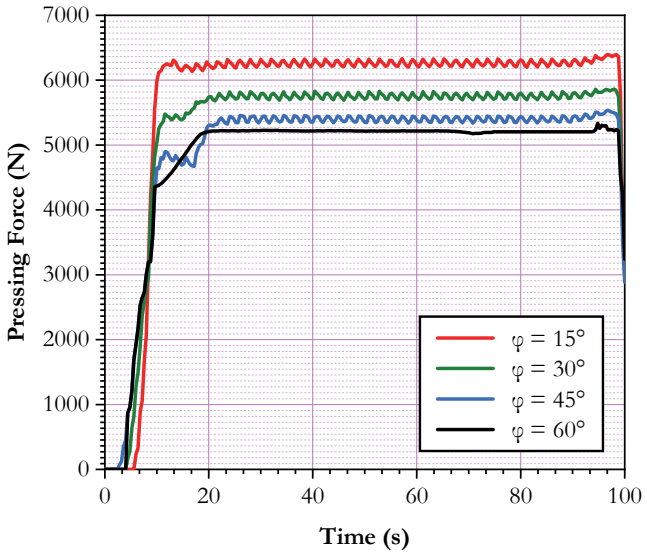

Figure 8: Numerical prediction of pressing force for different channel angles in the case of a 105° 1-ECAE die.

Effect of friction

This section investigates the effect of friction on the pressing force and the equivalent plastic strain distribution in the 1-ECAE die with a corner angle of φ = 15°. The interaction between the billet and the die wall is modeled according to Coulomb's law, considering four friction coefficients: f = {0, 0.1, 0.2, 0.3}. Fig. 9 illustrates the evolution of the plastic strain distribution along the sample thickness.

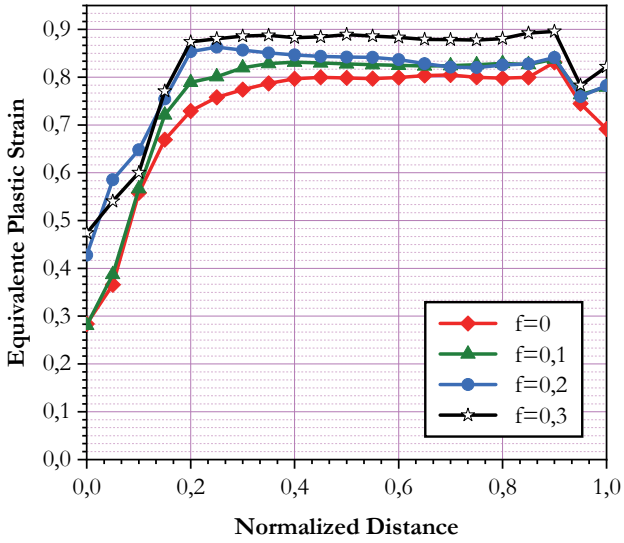

Figure 9: Illustration of the friction effect on the equivalent plastic strain distribution for φ = 15° in the case of 1-ECAE with a 105° die.

The results demonstrate that friction exerts a significant influence on both the intensity and the uniformity of plastic deformation. In the absence of friction (f = 0, red curve), the strain distribution is relatively low and homogeneous, indicating nearly ideal sliding conditions with limited resistance from the die walls. As the friction coefficient increases to 0.1, 0.2, and 0.3, a progressive rise in plastic strain is observed, especially near the inlet zone (normalized distance < 0.2), where shear localization becomes more pronounced. This increase is accompanied by a steeper slope at the entrance of the channel, reflecting accelerated deformation, followed by stabilization further along the cross-section. For instance, at f = 0.3 (black curve), the equivalent plastic strain exceeds 0.85, significantly higher than in the other cases, suggesting more constrained flow and improved strain homogenization across the section. Mechanistically, the additional resistance generated by friction forces the material to undergo more intense shear deformation to pass through the die channels. While moderate friction appears beneficial by enhancing strain development and homogenization, excessive friction may introduce drawbacks such as flow instabilities, defect formation, and accelerated die wear. Overall, these findings emphasize the crucial role of interfacial friction in the ECAE process, showing that its proper control is essential to optimize both the intensity and the uniformity of plastic strain distribution.

Case of a 105° 2-ECAE Die - Evolution of the plastic strain and the variation factor

Fig. 10 presents the equivalent plastic strain distribution for four different second-channel lengths, L = 20, 30, 40, and 50 mm, considering a section of 10 × 10 mm², and a corner angle of φ = 15°. The results reveal that the plastic strain distribution is generally non-uniform at the sample extremities. In contrast, a more homogeneous distribution is observed in the central region. Furthermore, the folding phenomenon appears markedly more pronounced when the second-channel length is short (L = 20 mm), indicating that a reduced channel length amplifies strain localization and flow instabilities.

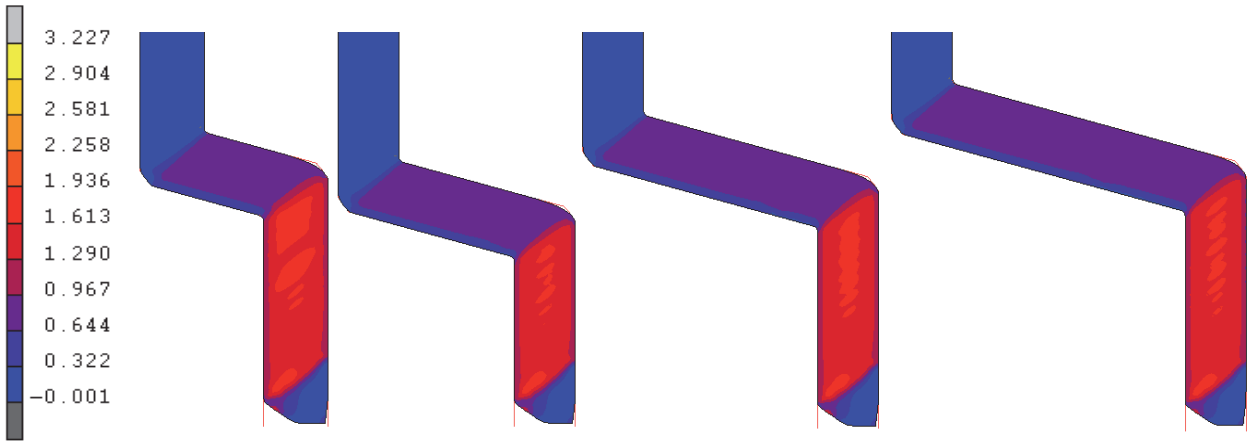

Figure 10: Equivalent plastic strain contours for polyamide during the 2-ECAE process with a 105° die at different second-channel lengths (L = 20, 30, 40, and 50 mm) for φ = 15°.

For more clarity, Fig. 11 illustrates the distribution of the equivalent plastic strain as a function of the distance from the bottom along the selected cross-section of the sample (see Fig. 4(b)), for each corner angle and for different second-channel lengths. The results clearly show that the highest plastic strain levels are obtained at a corner angle of φ = 15°, consistently across all tested channel lengths (L = 20, 30, 40, and 50 mm). In contrast, the lowest plastic strain values are observed for φ = 60°. This suggests that the corner angle φ has a predominant influence on the intensity of plastic deformation, while the second-channel length mainly affects the homogeneity of strain distribution.

In order to highlight the effect of the second channel length, the equivalent plastic strain along the selected section has been plotted for different lengths and for φ = 15° as shown in Fig. 12. It can be seen that the highest level of plastic strain is obtained for L=20 and 30 mm, however, for L=40 and 50 mm a slight difference has been observed.

The average equivalent plastic strain values obtained from the numerical simulations, along with the corresponding variation factors for the different geometries, are summarized in Tab. 3. It can be observed that the average plastic strain ranges between 1.24 and 1.52 across all cases. However, the results indicate that the most homogeneous strain distribution is achieved when the inner angle is φ = 15° and for a channel length L = 20 mm. This suggests that shorter channel lengths facilitate a more balanced redistribution of strain, thereby enhancing microstructural uniformity. Consequently, the

configuration with L = 20 mm proves to be the most favorable, as it minimizes strain localization while promoting overall homogeneity in the material.

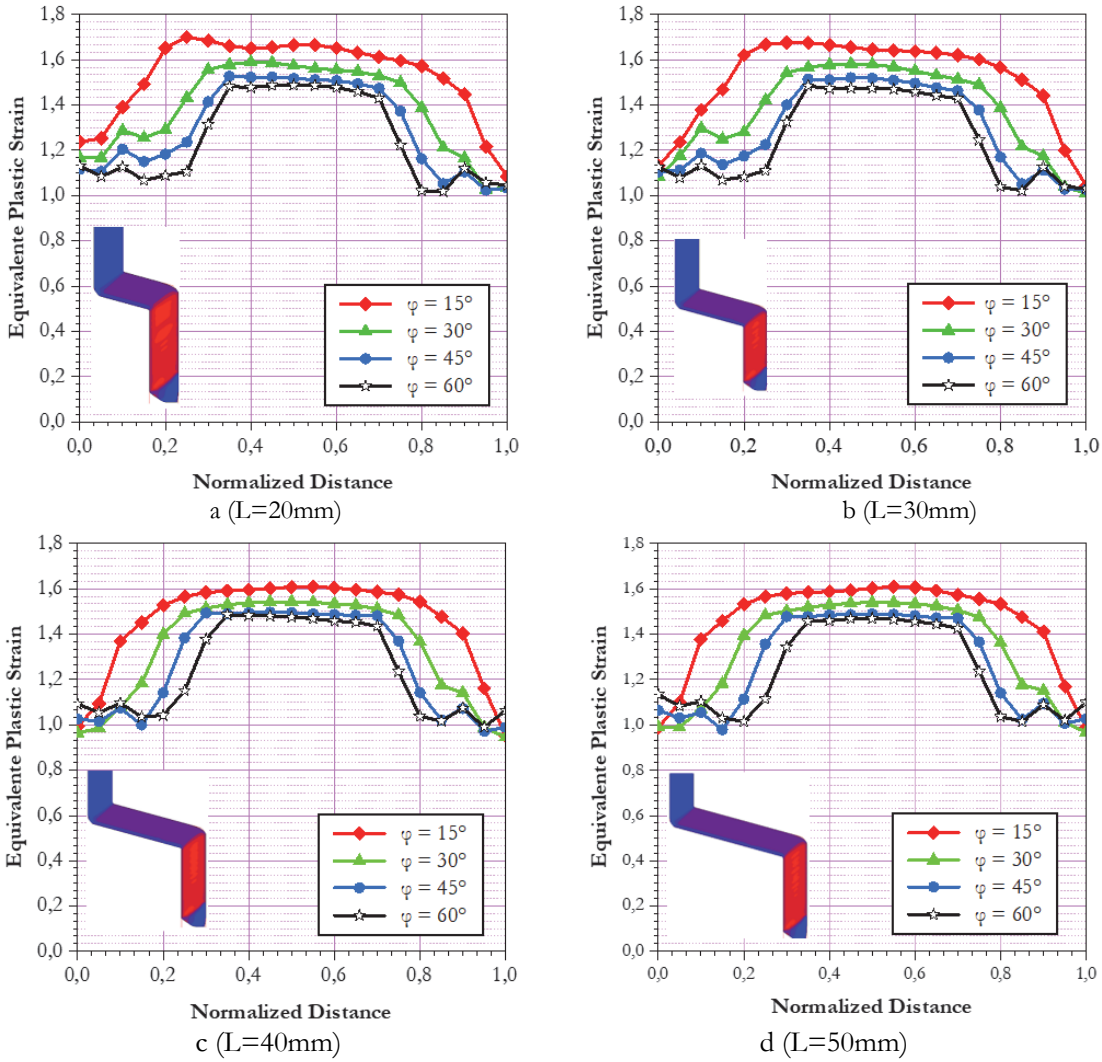

Figure 11: Distribution of the equivalent plastic strain along the selected cross-section (20 mm) for different corner angles in the case of the 105° 2-ECAE die.

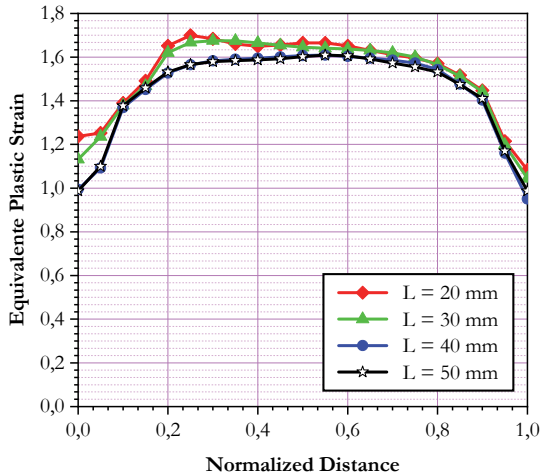

Figure 12: Distribution of the equivalent plastic strain along the selected cross-section for φ = 15° at different channel lengths in the case of the 105° 2-ECAE die.

	L (mm)	Maximum strain ε_{max}	Average strain ε_{ave}	Minimum strain ε_{min}	Variation factor V (%)
φ =15°	20	1.70	1.52	1.08	11.8
	30	1.68	1.51	1.04	12.8
	40	1.61	1.45	0.951	14.4
	50	1.61	1.45	0.987	13.9
φ =30°	20	1.59	1.38	1.03	13.8
	30	1.58	1.37	1.01	14.1
	40	1.54	1.33	0.945	17.0
	50	1.54	1.33	0.967	16.4
φ =45°	20	1.53	1.30	1.02	14.6
	30	1.52	1.29	1.03	14.5
	40	1.50	1.27	0.972	17.2
	50	1.49	1.27	0.979	16.4
φ =60°	20	1.49	1.25	1.02	15.1
	30	1.48	1.24	1.02	14.8
	40	1.49	1.24	0.99	15.9
	50	1.47	1.24	1.01	15.1

Table 3: Evolution of the equivalent plastic strain and variation factor as a function of φ and L for the 105° die in the 2-ECAE process.

Evolution of the pressing force

The magnitude of the pressing force required to extrude the sample is a key factor in defining the practical operating limits of the ECAE device. In this study, the pressing force for polyamide (PA) extrusion was numerically determined by evaluating the nodal reaction forces applied at the top surface of the sample during the process. Fig. 13 illustrates the temporal evolution of this force for a cross-section of 10 × 10 mm², considering various second-channel lengths and different corner angles (φ). It can be observed that the pressing force increases sharply at the initial stage of extrusion, corresponding to the onset of shear deformation at the die entrance. Once the sample passes through the elbows and establishes a steady-state flow, the force tends to stabilize. The magnitude of the force is strongly influenced by both the channel length and the corner angle, with sharper angles generally requiring higher pressing forces due to the more pronounced shear localization. These results highlight the trade-off between achieving higher plastic strain levels and maintaining manageable pressing forces, which is crucial for the practical design and optimization of ECAE dies.

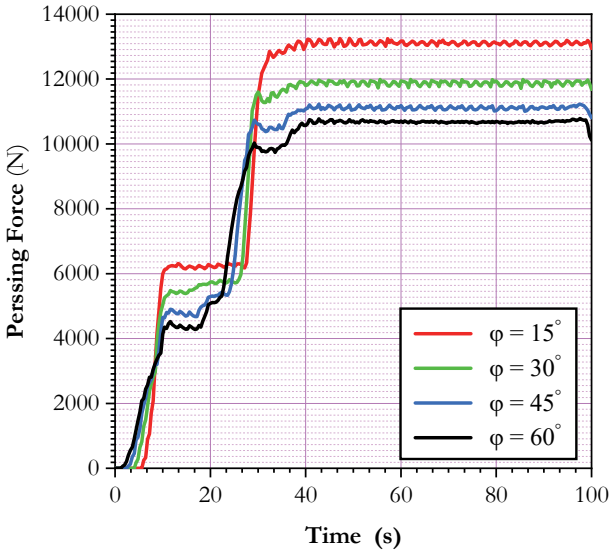

(a) L=20mm

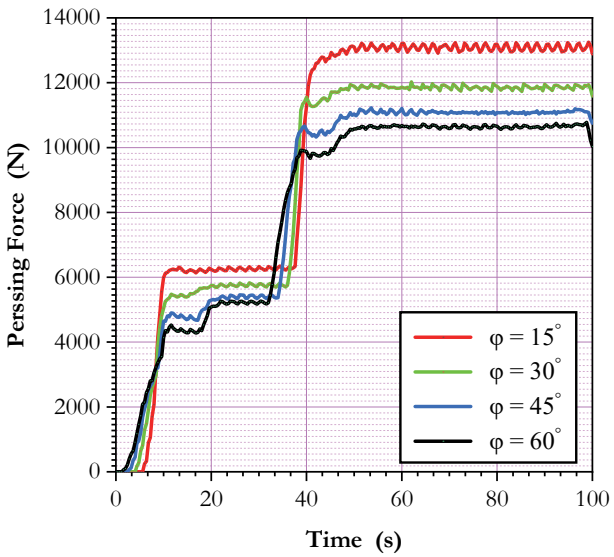

(b) L=30mm

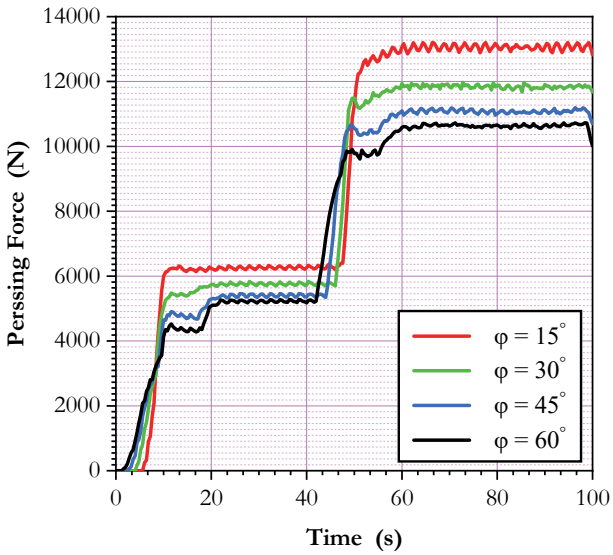

(c) L=40mm

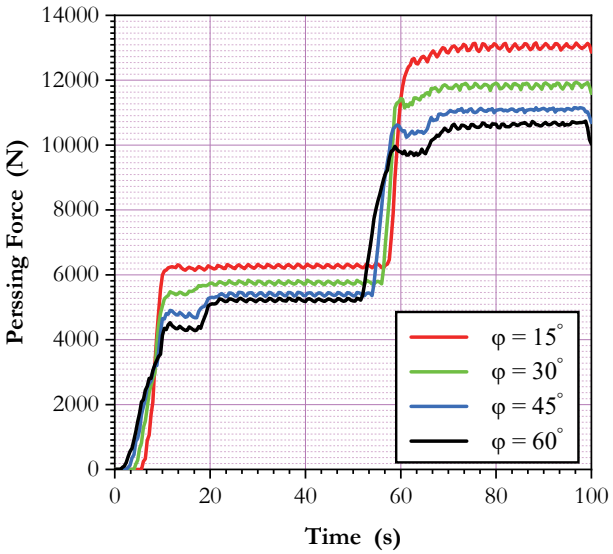

(d) L=50mm

Figure 13: Variation of the pressing force for different channel angles in the case of the 105° 2-ECAE die.

The maximum punch force obtained from the numerical simulations for the different die geometries is summarized in Tab. 4. It can be observed that the maximum punch force increases as the second-channel corner angle decreases. Overall, the required force ranges between 10.7295 kN and 13.2554 kN across all configurations. Notably, the most homogeneous plastic strain distribution was achieved at a maximum pressing force of 13.2554 kN, corresponding to a channel length of L = 20 mm and a corner angle of φ = 15°. However, the reduced maximum pressing force (approximately 10.73 kN) was obtained for φ = 60° and L = 40 mm (see Tab. 4 and Fig. 14).

	L (mm)	Maximum punch force required (kN)
φ =15°	20	13.2554
	30	13.2489
	40	13.2090
	50	13.1520
φ =30°	20	11.9885
	30	12.0265
	40	11.9711
	50	11.9382
φ =45°	20	11.2298
	30	11.2240
	40	11.1924
	50	11.1540
φ =60°	20	10.7836
	30	10.7751
	40	10.7295
	50	10.7383

Table 4: Numerical evolution of the punch force as a function of φ and L in the case of the 105° 2-ECAE die.

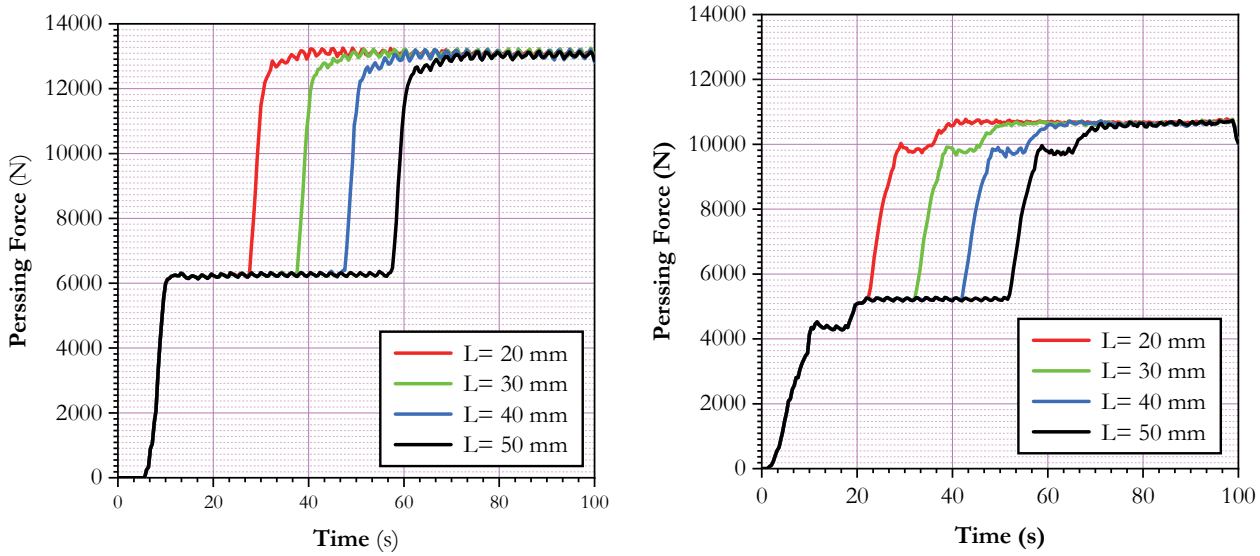

Figure 14: Variation of the pressing force for different channel lengths at φ = 15° and φ = 60° in the case of 2-ECAE using a 105° die.

At the onset of extrusion, the pressing force begins to rise as the material comes into contact with the first outer corner of the second channel. At this stage, the initiation and subsequent growth of a shear band occur until the sample head fully passes through the first elbow, corresponding to the first plastic deformation zone. The curve then reaches a first plateau, which reflects the steady-state plastic flow as the material traverses this elbow. Upon crossing the second plastic deformation zone, a second plateau with slight undulations appears, attributable to the interaction between the plastic deformations generated by both elbows of the die.

Effect of friction - Evolution of the equivalent plastic strain

In this section, the effects of friction on the equivalent plastic strain distribution and the pressing force are analyzed for the optimized geometries of a 105° 2-ECAE die with φ = 15° and L = {20, 30, 40, 50 mm}. The interaction between the tool and the billet is modeled using Coulomb's law of friction, and numerical simulations were conducted with four friction coefficients: f = {0, 0.1, 0.2, 0.3}.

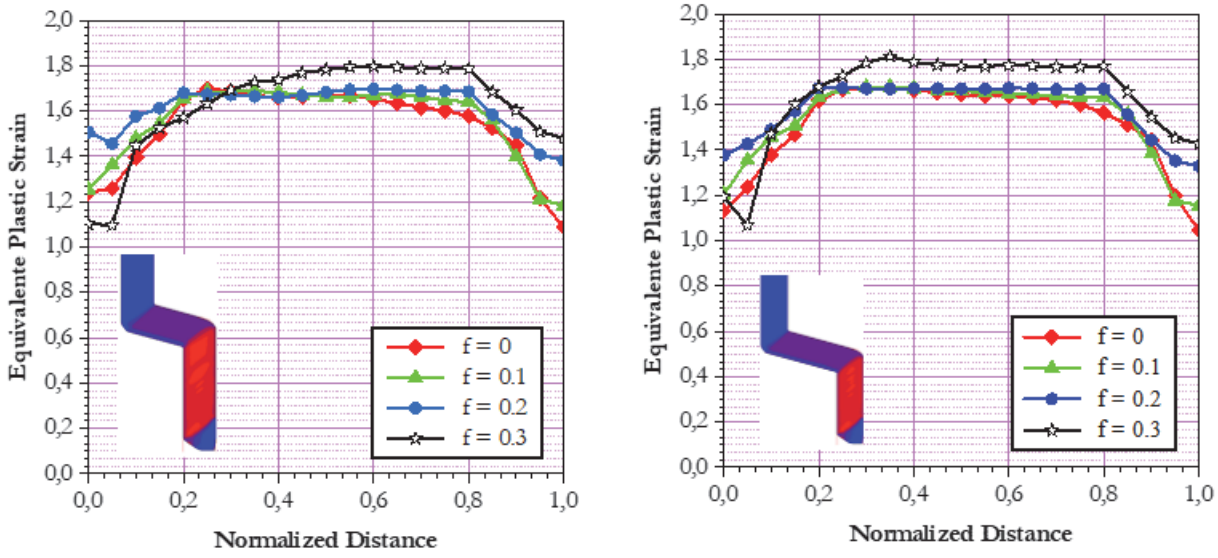

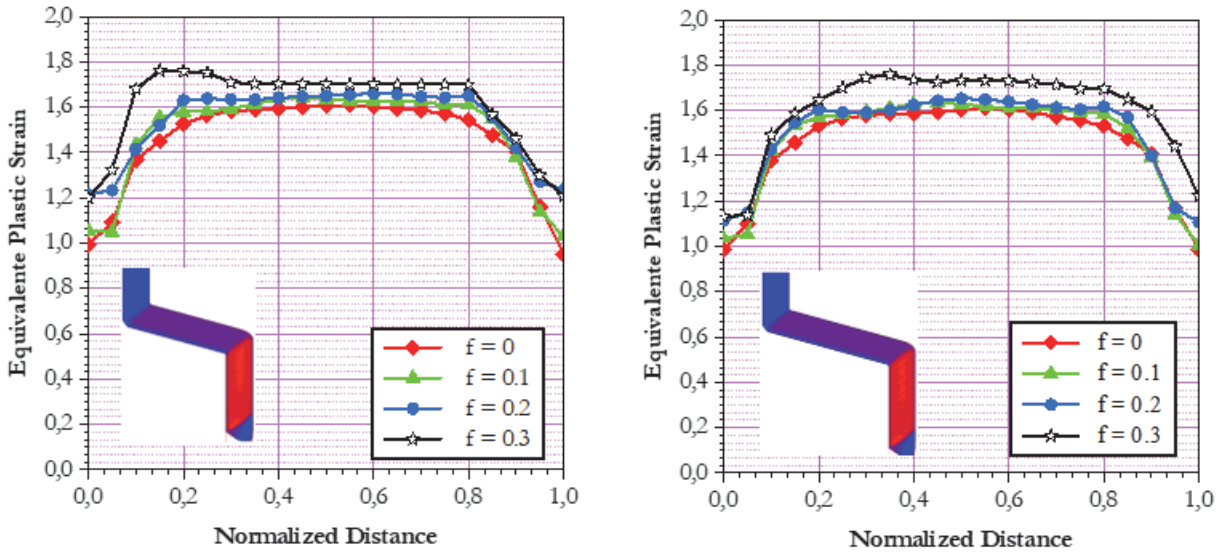

(c) L=40mm (d) L=50mm

Figure 15: Illustration of the friction effect on the equivalent plastic strain distribution in the case of 105° die 2-ECAE.

Fig. 15 presents the distribution of equivalent plastic strain across the sample for different lengths of the second channel. The results indicate that, under this configuration, friction exerts only a moderate influence on the homogeneity of strain distribution. However, as the friction coefficient increases, localized strain intensification tends to occur near the die walls, which may adversely affect deformation uniformity. From a practical standpoint, extrusion can be carried out without lubrication, particularly at low friction levels, but the use of a suitable lubricant is strongly recommended. Lubrication not only promotes a more homogeneous strain distribution but also reduces tool wear, minimizes the risk of surface defects, and ensures greater stability of the material flow during extrusion. Consequently, appropriate friction management becomes a critical parameter in achieving both microstructural refinement and long-term tool durability in the ECAE process.

It is observed that friction has a significant impact on both the homogeneity and the magnitude of the equivalent plastic strain in the extruded polyamide (PA). Specifically, as the friction coefficient increases, the plastic strain also rises. To illustrate this effect, Fig. 16 presents the equivalent plastic strain contours for extrusion lengths L = 30 mm and L = 50 mm under different friction coefficients, where the color variations correspond to different strain levels. These results reveal the classical features of the ECAE process, emphasizing the role of friction in amplifying strain localization. Therefore, it is recommended to minimize friction as much as possible in order to prevent the initiation of micro-cracks at the billet–die interface and to ensure a more uniform strain distribution.

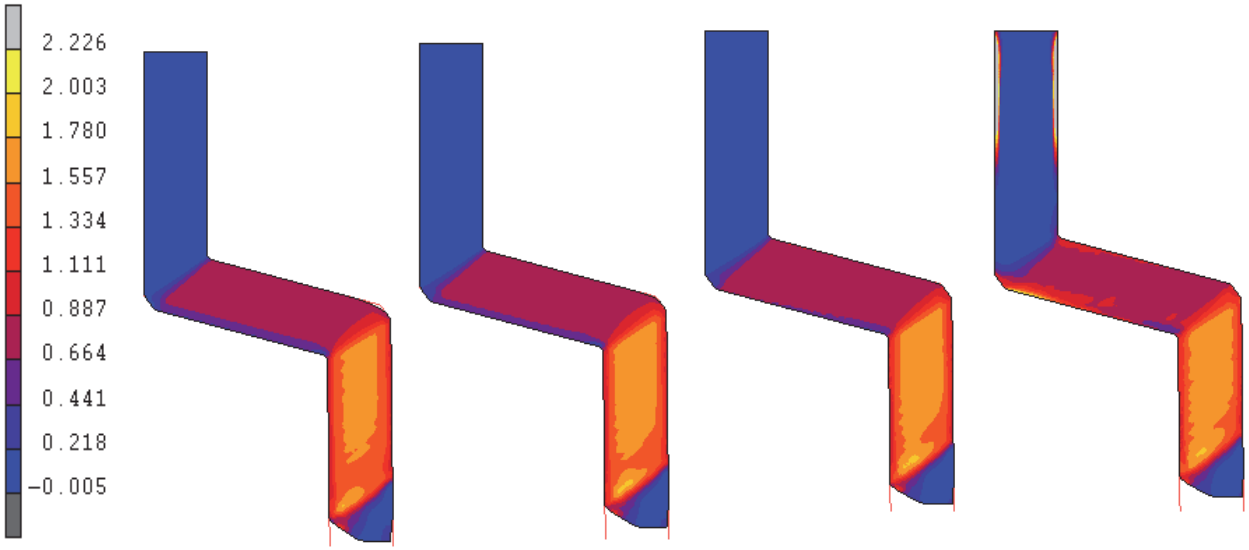

(a)

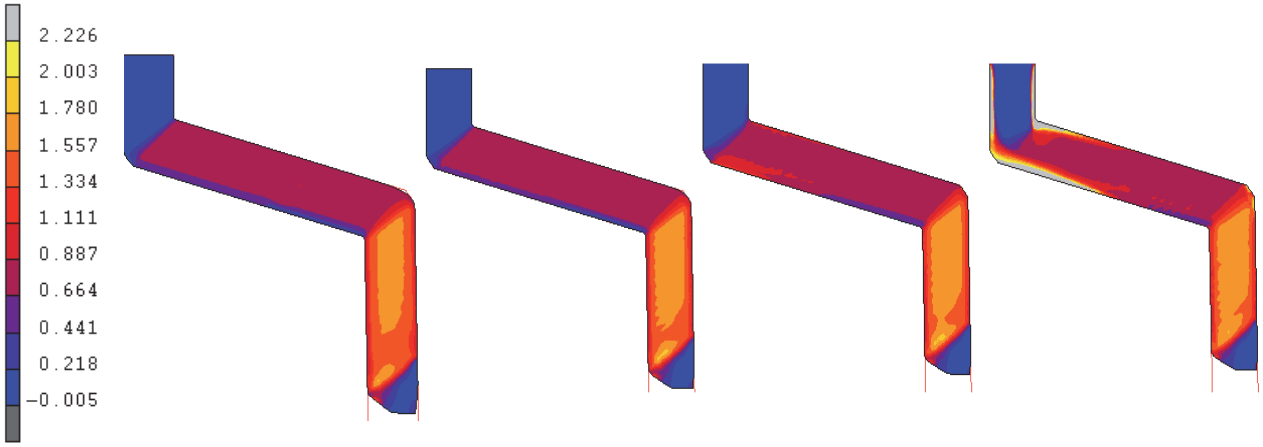

(b)

Figure 16: Equivalent plastic strain contours for polyamide during the 2-ECAE process using a 105° die at φ = 15° for different friction coefficients, with lengths: (a) L = 30 mm and (b) L = 50 mm.

Evolution of the variation factor

Fig. 17 presents the evolution of the variation factor for different friction coefficients in the case of the 105° 2-ECAE die. The results clearly demonstrate that friction has a significant impact on the homogeneity of the equivalent plastic strain distribution. The numerical values of the variation factor and the average equivalent plastic strain are summarized in Tab. 5. It can be observed that the average plastic strain varies between 1.45 and 1.64 across all studied cases, indicating a relatively high level of deformation. However, the variation factor, which reflects the degree of strain heterogeneity, exhibits its maximum values when friction is absent (f = 0) for all channel lengths. This outcome suggests that, in the absence of interfacial resistance, the material flow is less constrained, leading to uneven strain localization. Conversely, a moderate friction coefficient, particularly f = 0.2, appears to promote better strain homogenization, as evidenced by the lowest value of the variation factor obtained for L = 20 mm. This behavior can be explained by the fact that a controlled amount of friction enhances shear transfer between the die and the billet, thereby redistributing deformation more uniformly across the sample cross-section. Nevertheless, excessive friction (f = 0.3) tends to elevate strain levels but at the expense of introducing localized heterogeneities and potential risks of surface defects. These findings highlight the dual role of friction in the ECAE process: while a complete absence of friction induces non-uniform strain fields, a moderate coefficient can improve homogeneity, whereas excessive values may degrade material quality.

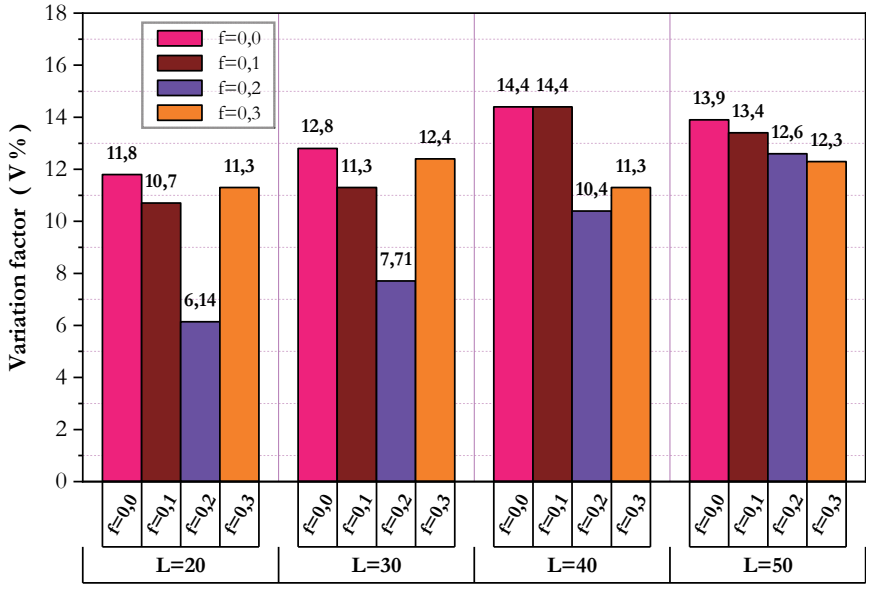

Figure 17: Illustration of the variation factor in the case of the 105° die 2-ECAE with the effect of friction.

Lengths of the second channel (mm)	Friction Coefficient f	Maximum strain ε_{max}	Average strain ε_{ave}	Minimum strain ε_{min}	Varition factor V (%)
L=20	0	1.70	1.53	1.09	11.8
	0.1	1.69	1.56	1.18	10.7
	0.2	1.7	1.61	1.38	6.14
	0.3	1.76	1.6	1.13	11.3
L=30	0	1.68	1.51	1.04	12.8
	0.1	1.68	1.54	1.16	11.3
	0.2	1.68	1.58	1.33	7.71
	0.3	1.81	1.64	1.07	12.4
L=40	0	1.61	1.45	0.951	14.4
	0.1	1.64	1.49	1.03	14.4
	0.2	1.66	1.54	1.22	10.4
	0.3	1.76	1.61	1.2	11.3
L=50	0	1.61	1.45	0.987	13.9
	0.1	1.63	1.48	1.01	13.4
	0.2	1.65	1.5	1.11	12.6
	0.3	1.76	1.6	1.13	12.3

Table 5: Evolution of the punch force, equivalent plastic strain, and variation factor as a function of L and f for an inner angle φ = 15° in the case of the 105° die 2-ECAE.

Evolution of pressing force

The evolution of the pressing force as a function of time for different channel lengths and friction conditions is presented in Fig. 18. It is evident that the maximum punch force increases with the rise in the friction coefficient, reflecting the additional resistance introduced at the billet–die interface. Quantitatively, the maximum pressing force varies between 13.1520 kN and 86.6768 kN for all simulated cases (see Tab. 6).

This trend is consistent with the mechanics of the ECAE process, where higher friction enhances energy dissipation and impedes smooth sliding of the material along the die walls, thereby requiring greater extrusion loads. However, excessive friction may also promote flow localization, leading to non-uniform strain fields and potential surface damage. Interestingly, the analysis shows that the most homogeneous plastic strain distribution was obtained when the pressing force reached 50.4739 kN, corresponding to a channel length of L = 20 mm and a friction coefficient of f = 0.2. This result highlights the critical balance between applied load and strain uniformity: moderate friction levels contribute to improved strain homogenization without excessively increasing the extrusion force. Consequently, this case can be considered as an optimal compromise between mechanical efficiency and microstructural refinement.

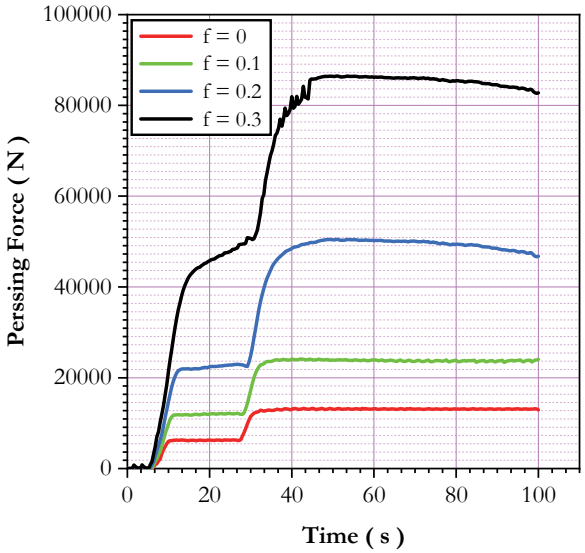

(a) L=20mm

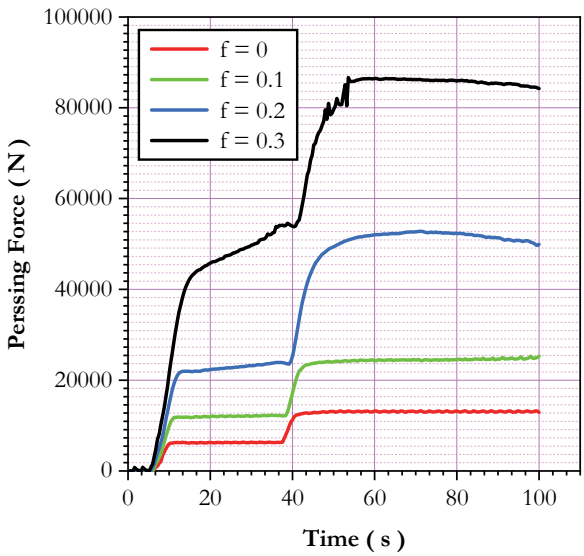

(b) L=30mm

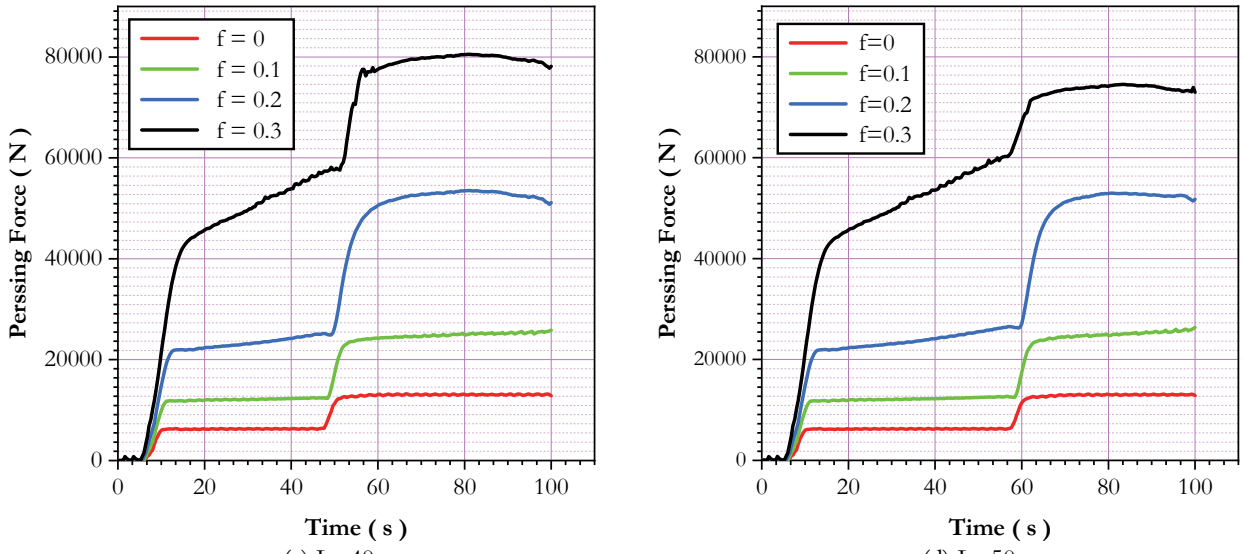

(c) L=40mm (d) L=50mm

Figure 18: Illustration of the friction effect on the pressing force required for different channel lengths in the case of the 105° die 2-ECAE for different lengths of the second channel.

	L (mm)	Maximum punch force required (kN)
f=0	20	13.2554
	30	13.2489
	40	13.2090
	50	13.1520
f=0.1	20	24.1072
	30	25.2834
	40	25.8381
	50	26.3791
f=0.2	20	50.4739
	30	52.823
	40	53.5339
	50	52.9771
f=0.3	20	86.4739
	30	86.6768
	40	80.5339
	50	64.5339

Table 6: Evolution of the punch force as a function of the variation factor in the case of the 105° die 2-ECAE.

EXPERIMENTAL TESTS OF ECAE

Based on the optimization of the geometric parameters, a 2-ECAE die was designed and fabricated with a channel angle of 105°, a square cross-section of 10 × 10 mm, and an intermediate channel length of 20 mm (Fig. 19(a)). To enable a meaningful comparison and to assess the influence of multiple elbows on the deformation behavior, a complementary 1-ECAE die with a single elbow and the same channel angle was also designed and manufactured (Fig. 19(b)). For both dies, the entrance and exit channel lengths were fixed at 108 mm and 97 mm, respectively, ensuring comparable flow conditions. The billets processed in both configurations had a square cross-section of 10 × 10 mm with a slight clearance fit relative to the die walls, allowing a direct evaluation of the effect of die geometry, specifically the number of elbows, on curvature evolution and mechanical properties.

The investigated material was polyamide (PA 6.6), selected for its availability and semicrystalline microstructure. The samples, with a typical length of 85–100 mm and a cross-section not exceeding 10 × 10 mm², were machined along the

same direction from a polyamide plate of dimensions 10 mm (thickness) × 1000 mm × 1000 mm supplied by COTIMET (Algeria). The billets were simultaneously surfaced on the cutting faces using a three-size milling cutter and polished to the final dimensions. Prior to extrusion, all samples were annealed at 108 °C for 6 h and slowly cooled inside the furnace to room temperature to eliminate pre-existing thermal history and residual stresses. The extrusion experiments were carried out using a hydraulic press, with sufficiently lubricated die channels to minimize friction during processing. A constant ram speed of 0.07 mm/s was maintained to ensure quasi-static loading conditions and reproducibility of the results across different die configurations.

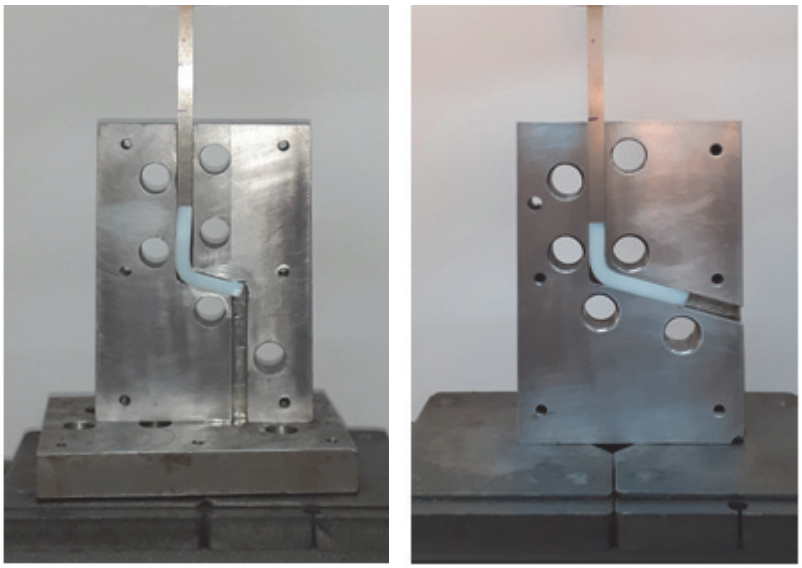

(a) (b)

Figure 19: Experimental study of the polyamide behavior using a 105° die with: (a) two elbows (2-ECAE) and (b) one elbow (1-ECAE).

Evolution of curvature

A polyamide (PA 6.6) plate with initial dimensions of 1000 × 1000 × 12 mm³ was first sectioned. The obtained specimens were subsequently machined using a milling machine to reach approximate final dimensions of 10 × 10 × 85 mm³, with minor adjustments applied to ensure dimensional accuracy. The channel and sample widths and thicknesses were designed to be identical, while maintaining a clearance fit to enable proper extrusion without excessive friction. All ECAE experiments were performed under controlled conditions at room temperature (25 °C), with a constant ram speed of 0.07 mm/s. This value was selected to guarantee quasi-static loading conditions and to minimize thermal effects during deformation. These controlled parameters were chosen to ensure the reproducibility of the tests and to enable a reliable comparison of the results between different geometrical configurations.

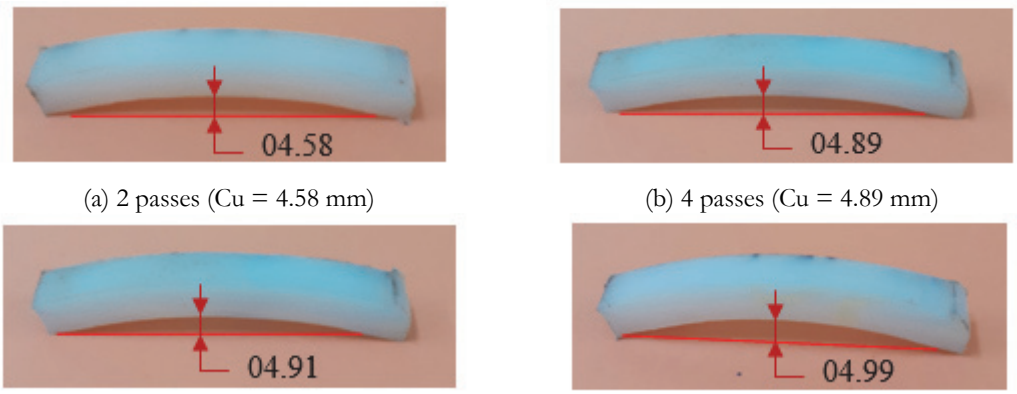

(a) 2 passes (Cu = 4.58 mm) (b) 4 passes (Cu = 4.89 mm)

(c) 8 passes (Cu = 4.91 mm) (d) 16 passes (Cu = 4.99 mm)

Figure 20: PA 6.6 samples extruded at room temperature after 2, 4, 8, and 16 passes using a 1-ECAE die with a 105° channel angle under Route C.

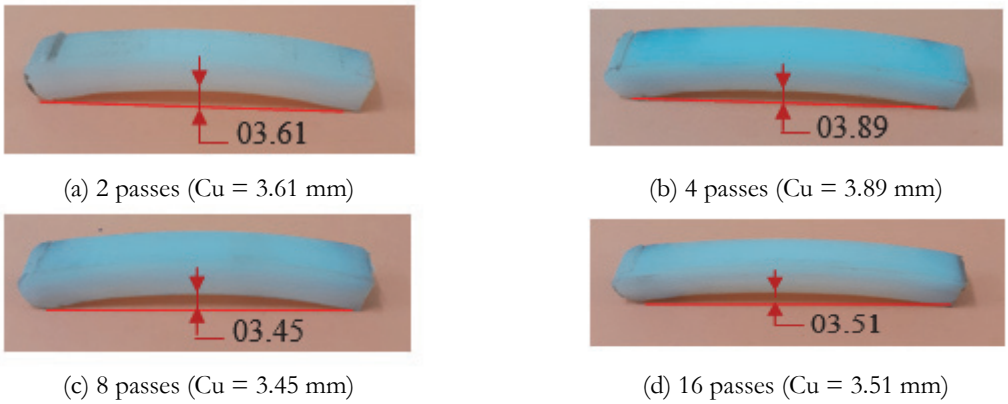

(a) 2 passes (Cu = 3.61 mm) (b) 4 passes (Cu = 3.89 mm)

(c) 8 passes (Cu = 3.45 mm) (d) 16 passes (Cu = 3.51 mm)

Figure 21: PA 6.6 samples extruded at room temperature after 2, 4, 8, and 16 passes using a 2-ECAP die with a 105° channel angle under Route C.

The warping behavior of the extruded samples produced with both 1-ECAE and 2-ECAE dies, following routes A and C, was evaluated in this experimental section. It should be recalled that route C involves a 180° rotation of the sample after each pass. Fig. 19 shows images of polyamide specimens subjected to one pass with both 1-ECAE and 2-ECAE dies, as well as four passes with the 1-ECAE die and two passes with the 2-ECAE die. The corresponding results are summarized in Tab. 7 and illustrated in Figs. 20 and 21. The maximum curvature (warping) of the samples was determined by comparing their height before and after extrusion. The results clearly indicate that, for an equivalent number of passes through the elbows, the 2-ECAE die consistently generates less warping than the 1-ECAE die. Notably, the curvature observed after two passes with the 2-ECAE die is less than half of that obtained after four passes with the 1-ECAE die, highlighting the superior dimensional stability of the 2-ECAE configuration.

	N° Passe	Height before extrusion H_1 (mm)	Height after extrusion H_2 (mm)	Curvature $C_u = H_2 - H_1$ (mm)
1-ECAE die with route A	1	9.50	14.85	5.35
	2	9.53	15.81	6.28
	3	9.53	15.93	6.40
	4	9.43	16.13	6.70
	8	9.45	16.75	7.30
	12	9.78	17.63	7.85
	16	9.15	17.17	8.02
1-ECAE die with route C	1	9.60	14.10	4.50
	2	9.58	14.16	4.58
	3	9.98	14.76	4.78
	4	9.70	14.89	4.89
	8	10.00	14.91	4.91
	12	9.43	14.38	4.95
	16	9.48	14.47	4.99
2-ECAE die with route C	2	9.89	13.50	3.61
	4	9.78	13.67	3.89
	8	9.70	13.15	3.45
	16	9.71	13.22	3.51

Table 7: Curvature values of polyamide samples processed with 1-ECAE and 2-ECAE dies using a 105° channel angle under Routes A and C.

Fig. 22 illustrates the evolution of curvature as a function of the number of passes at room temperature for 1-ECAE and 2-ECAE dies with a 105° channel angle using Routes A and C. It can be observed that the 1-ECAE configuration with Route A leads to a continuous and pronounced increase in curvature, reaching nearly 8 mm after 16 passes. This behavior indicates strong strain localization and the progressive accumulation of residual stresses, which are typical of this processing route. In contrast, 1-ECAE with Route C shows a much more moderate evolution, with curvature stabilizing around 5 mm after the first few passes, suggesting improved stress redistribution due to the alternating rotations. The 2-ECAE configuration with Route C exhibits the lowest curvature values, remaining between 3 and 3.5 mm even after 16 passes. This result confirms that the two-turn die geometry significantly reduces the accumulation of non-uniform strain and limits excessive warping or bending of the samples.

Overall, the figure highlights that the combination of 2-ECAE with Route C is the most effective condition for minimizing curvature and enhancing strain homogeneity, whereas 1-ECAE Route A promotes a progressive increase in this defect. These findings emphasize the critical role of die geometry and processing route selection in controlling residual stresses and deformation behavior of polymers during ECAE processing.

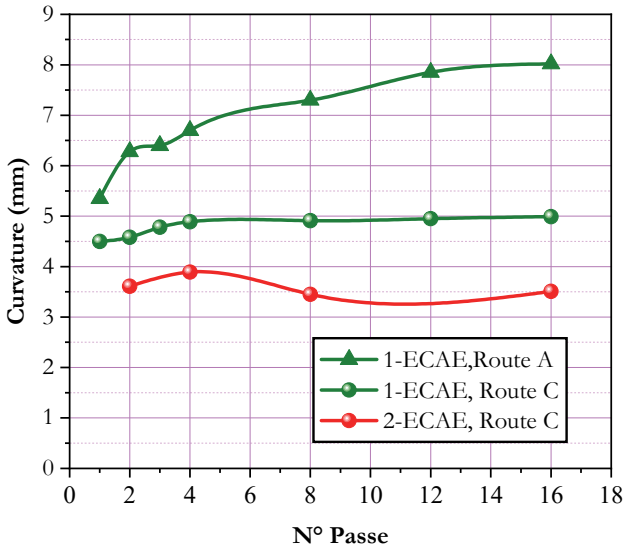

Figure 22: Evolution of curvature as a function of the number of passes at room temperature for 1-ECAE and 2-ECAE dies with a 105° channel angle, Routes A and C.

Evolution of hardness

Hardness measurements were conducted at room temperature using a Brinell hardness tester in order to evaluate the effect of the ECAE process on the mechanical properties of the polyamide samples. For each specimen, five indentation points were selected, positioned in an approximately equidistant manner across the surface, and the average value was calculated to minimize local variations. The evolution of the mean hardness values is presented in Tab. 8 and Fig. 23, for samples processed with 1-ECAE and 2-ECAE dies featuring a channel angle of 105°, following both Route A and Route C. The results clearly highlight the influence of the processing route on the material response: Route A generally promotes a gradual increase in hardness due to continuous strain accumulation, while Route C, by introducing sample rotations between passes, tends to provide more uniform hardening with reduced anisotropy. This comparison demonstrates the significant role of the chosen processing route in tailoring the mechanical performance of extruded materials.

The data show that hardness systematically increases with the number of passes, confirming the effect of strain hardening induced by the severe plastic deformation process. For the 1-ECAE die with Route A, hardness values exhibit a continuous and significant increase, rising from 8.99 HB at the first pass to 12.85 HB after 16 passes. This steady trend reflects progressive strain accumulation and high dislocation density, characteristic of Route A processing.

In contrast, the 1-ECAE die with Route C shows a different behavior: while hardness initially increases (from 8.73 HB to about 10.99 HB after 8 passes), the values stabilize thereafter and even slightly decrease to 10.43 HB after 16 passes. This indicates that Route C promotes faster saturation of hardening, likely due to texture disruption and refinement mechanisms that limit further dislocation accumulation.

The 2-ECAE configuration with Route C achieves intermediate hardness values, starting at 9.77 HB after 2 passes and peaking at 11.48 HB after 8 passes, before slightly decreasing to 11.57 HB at 16 passes. This suggests that the two-step

geometry enhances strain distribution and reduces localized deformation, leading to a more moderate but stable hardening effect compared to the single-step die.

Overall, these results highlight that the 1-ECAE Route A condition is most effective in maximizing hardness through continuous strain accumulation, while Route C and the 2-ECAE die configurations promote more balanced hardening behavior with reduced risk of overstraining or material relaxation. This demonstrates the crucial role of die geometry and processing route in tailoring the mechanical performance of polymers during ECAE.

N° Passe	1-ECAE (Route A) (HB)	1-ECAE (Route C) (HB)	2-ECAE (Route C) (HB)
1	8.99	8.73	
2	9.22	8.97	9.77
3	9.67	9.26	
4	10.04	10.06	10.62
8	11.69	10.99	11.48
12	12.42	10.73	
16	12.85	10.43	11.57

Table 8: Values of hardness average of polyamide samples obtained by 1-ECAE and 2-ECAE dies with a channel angle of 105° with route A and route C.

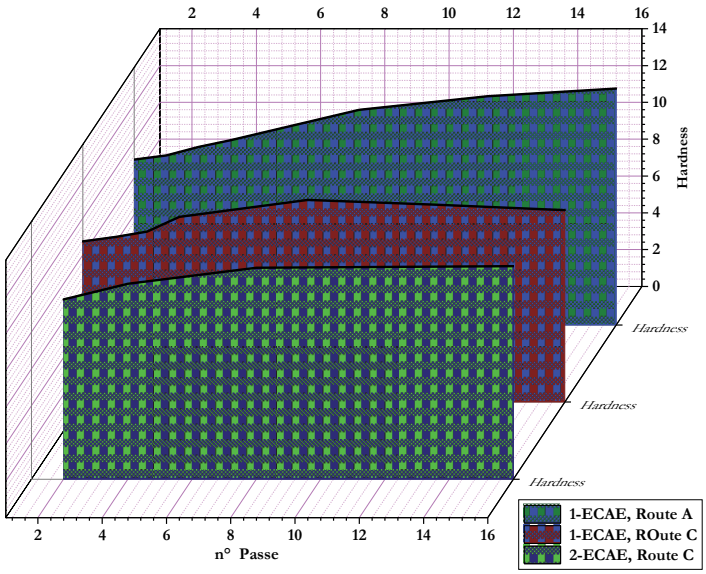

Figure 23: Evolution of hardness as a function of the number of passes at room temperature using a 1-ECAE and 2-ECAE die with a 105° channel angle, Routes A and C.

CONCLUSION

This study was structured into two complementary parts combining numerical and experimental approaches. The first part focused on the numerical modeling and optimization of the geometric and processing parameters of the ECAE process, which provided the basis for the design and fabrication of ECAE dies with one and two channels. The second part was devoted to the experimental investigation of the material response, with particular emphasis on the evolution of curvature and hardness as indicators of deformation homogeneity and mechanical strengthening. Overall, the results highlight the crucial role of die geometry, corner angle, friction conditions, and processing routes in governing the deformation behavior of polyamide (PA) during equal channel angular extrusion (ECAE) using a 105° die. Based on these findings, the following conclusions can be drawn:

Analytical and finite element analyses demonstrated that sharper corner angles intensify plastic strain but compromise strain homogeneity, whereas optimized geometries (φ = 15° and L = 20 mm) provide a better balance by improving uniformity and reducing the warping phenomenon.

Friction exerts a moderate influence on strain distribution and pressing force in the 105° ECAE die. While low friction levels maintain acceptable homogeneity, higher coefficients lead to localized strain near the die walls and potential surface defects. Lubrication is thus recommended to improve deformation uniformity, reduce tool wear, and ensure stable material flow, making friction control a critical factor for optimized ECAE performance.

Experimental results further confirmed the numerical predictions, showing that the 2-ECAE configuration effectively reduces curvature and enhances strain homogeneity compared to the 1-ECAE die, particularly when combined with Route C. In addition, hardness measurements revealed that mechanical performance can be tailored through the number of passes and processing routes. Taken together, these findings demonstrate that careful optimization of ECAE parameters enables more uniform strain distribution, minimized warping, and enhanced mechanical properties of polymers, thereby supporting the broader industrial application of ECAE-processed polymeric materials.

As a perspective, a systematic comparison between numerical predictions and experimentally measured force–time curves will be carried out in future work currently under development. This experimental–numerical confrontation will allow a quantitative validation of the proposed model and further assessment of its predictive capability, particularly with respect to force evolution and material response during the ECAE process.

REFERENCES

[1] Segal, V. M. (1995). Materials processing by simple shear. Mater. Sci. Eng.: A, 197(2), pp. 157–164. DOI: https://doi.org/10.1016/0921-5093(95)09705-8.

[2] Lee, S., Berbon, P. B., Furukawa, M., Horita, Z., Nemoto, M., Tsenev, N. K., Valiev, R. Z. and Langdon, T. G. (1999). Developing superplastic properties in an aluminum alloy through severe plastic deformation. Mater. Sci. Eng.: A, 272(1), pp. 63–72. DOI: https://doi.org/10.1016/S0921-5093(99)00470-0.

[3] Kim, H. S. and Estrin, Y. (2005). Microstructural modelling of equal channel angular pressing for producing ultrafine grained materials. Mater. Sci. Eng.: A, 410–411, pp. 285–289. DOI: https://doi.org/10.1016/j.msea.2005.08.047.

[4] Sue, H. J. and Li, C. K. Y. (1998). Control of orientation of lamellar structure in linear low-density polyethylene via a novel equal channel angular extrusion process. J. Mater. Sci. Lett., 17(10), pp. 853–856. DOI: https://doi.org/10.1023/A:1006659127256.

[5] Zaïri, F., Aour, B., Gloaguen, J. M., Naït-Abdelaziz, M. and Lefebvre, J. M. (2008). Steady plastic flow of a polymer during ECAE process: Experiments and numerical modeling. Polym. Eng. Sci., 48(5), 1015–1021. DOI: https://doi.org/10.1002/pen.21042.

[6] Aour, B., Zaïri, F., Gloaguen, J. M., Naït-Abdelaziz, M. and Lefebvre, J. M. (2009). Finite element analysis of plastic strain distribution in multi-pass ECAE process of high-density polyethylene. J. Manuf. Sci. Eng., 131(3), 031016. DOI: https://doi.org/10.1115/1.3139217.

[7] Park, S. H. (2015). Derivation of fatigue properties of plastics and life prediction for plastic parts. Proceedings of the 2015 World Congress on Advances in Civil, Environ. Mater. Res. (ACEM 15), Incheon, Korea.

[8] Sue, H. J., Dilan, H. and Li, C. K. Y. (1999). Simple shear plastic deformation behavior of polycarbonate plate due to the equal channel angular extrusion process. I: Finite element modeling. Polym. Eng. Sci., 39(12), pp. 2505–2515. DOI: https://doi.org/10.1002/pen.11638.

[9] Li, C. K. Y., Xia, Z. Y. and Sue, H. J. (2000). Simple shear plastic deformation behavior of polycarbonate plate. II: Mechanical property characterization. Polym., 41(16), pp. 6285–6293. DOI: https://doi.org/10.1016/S0032-3861(99)00837-X.

[10] Xia, Z., Sue, H. J. and Hsieh, A. J. (2001). Impact fracture behavior of molecularly oriented polycarbonate sheets. J. Appl. Polym. Sci., 79(11), pp. 2060–2066. DOI: https://doi.org/10.1002/1097-4628(20010314)79:11.

[11] Xia, Z., Sue, H. J., Hsieh, A. J. and Huang, J. W. L. (2001). Dynamic mechanical behavior of oriented semi-crystalline polyethylene terephthalate. J. Polym. Sci. B: Polym. Phys., 39(13), pp. 1394–1403. DOI: https://doi.org/10.1002/polb.1111.

[12] Weon, J. I., Creasy, T. S., Sue, H. J. and Hsieh, A. J. (2005). Mechanical behavior of polymethyl methacrylate with molecules oriented via simple shear. Mater. Sci. Eng., 45(3), pp. 314–324. DOI: https://doi.org/10.1002/pen.20269.

[13] Jiang, Q., Boulahia, R., Zaïri, F., Vozniak, I., Qu, Z., Gloaguen, J. and Liu, X. (2022). Microstructure and mechanical properties of severely deformed polypropylene in ECAE (equal channel angular extrusion) via routes A and C. Polym., 14(23), 5287. DOI: https://doi.org/10.3390/polym14235287.
[14] Beloshenko, V. B., Vozniak, A. V. and Voznyak, A. V. (2023). Equal channel angular extrusion of polymers: Structural changes and their effects on properties. Mater. Trans., 64(6), pp. 1325–1330. DOI: https://doi.org/10.2320/matertrans.MT-MF2022017
[15] Vasylevskyi, K. V., Tsukrov, I. T., Miroshnichenko, K. M., Buklovskyi, S. B., Grover, H. G. and Van Citters, D. V. C. (2021). Finite element model of equal channel angular extrusion of ultra-high molecular weight polyethylene. J. Manuf. Sci. Eng., 143(12), 121007. DOI: https://doi.org/10.1115/1.4051189.
[16] Weon, J. I. and Sue, H. J. (2005). Effects of clay orientation and aspect ratio on mechanical behavior of nylon-6 nanocomposites. Polym., 46(17), pp. 6325–6334. DOI: https://doi.org/10.1016/j.polymer.2005.05.094.
[17] Wang, Z. G., Xia, Z. Y., Yu, Z. Q., Chen, E. Q., Sue, H. J., Han, C. C. and Hsiao, B. S. (2006). Lamellar formation and relaxation in simple sheared polyethylene terephthalate) by small-angle X-ray scattering. Macromolecules, 39(8), pp. 2930–2939. DOI: https://doi.org/10.1021/ma051928k.
[18] Aour, B. and Mitsak, A. (2016). Analysis of plastic deformation of semi-crystalline polymers during ECAE process using 135° die bending. J. Theor. Appl. Mech., 54(1), pp. 263–275. DOI: https://doi.org/10.15632/jtam-pl.54.1.263.
[19] Segal, V. M. (1999). Equal channel angular extrusion: From macromechanics to structure formation. Mater. Sci. Eng.: A, 271(1–2), pp. 322–333. DOI: https://doi.org/10.1016/S0921-5093(99)00248-8.
[20] Beygelzimer, Y. E. and Beloshenko, V. A. (2004). Solid-state extrusion. In J. I. Kroschewitz (Ed.), Encyclopedia of Polymer Science and Technology. Hoboken, NJ, USA: John Wiley & Sons. DOI: https://doi.org/10.1002/0471440264.pst343.
[21] Lemaitre, J., and Chaboche, J.L. (1990). Mechanics of solid materials. Cambridge University Press. DOI: https://doi.org/10.1017/CBO9781139167970.
[22] Simo, J. C. and Hughes, T. J. R. (1998). Computational inelasticity. Springer. DOI : https://doi.org/10.1007/b98904.
[23] Perzyna, P. (1966). Fundamental problems in viscoplasticity. Adv. Appl. Mech., 9, pp. 243–377. DOI: https://doi.org/10.1016/S0065-2156(08)70009-7.
[24] Perzyna, P. (1963). The constitutive equations for rate-sensitive plastic materials. Q. Appl. Math., 20(4), pp. 321–332. DOI: https://doi.org/10.1090/qam/144536.
[25] Boyce, M. C., Parks, D. M. and Argon, A. S. (1988). Large inelastic deformation of glassy polymers. Part I: Rate-dependent constitutive model. Mech. Mater., 7(1), pp. 15–33. DOI: 10.1016/0167-6636(88)90003-8.
[26] Tervoort, T. A., Smit, R. J. M. and Govaert, L. E. (1998). A constitutive equation for the elasto-viscoplastic deformation of glassy polymers. J. Mech. Phys. Solids, 46(8), pp. 1379–1411. DOI: 10.1023/A:1009720708029.
[27] Voce, E. (1955). A practical strain-hardening function. Metallurgia, 51, pp. 219–226.
[28] Govaert, L. E. and Tervoort, T. A. (2017). Strain hardening in polymer glasses: On the definition of yield stress. J. Polym. Sci. B: Polym. Phys., 55(5), pp. 405–418. DOI: https://doi.org/10.1002/polb.24353.
[29] Xiao, Y., Wang, Z., Wang, R., Zhang, X., Fan, C., Wei, Z. and Sun, Y. (2022). A viscoelastic–viscoplastic constitutive model for polymeric materials under multiaxial stress states. Sci. Rep., 12, 7825. DOI: https://doi.org/10.1038/s41598-022-26525-z.
[30] Lenders, T., Langer, C., Chevalier, J., Kerschbaum, M., Hartmaier, A. and Wafai, H. (2023). An elasto-viscoplastic constitutive model for the rate-dependent behaviour of polymers. Mech. Mater., 181, 104565. DOI: https://doi.org/10.1016/j.mechmat.2023.104565.
[31] Johnsen, J., Høyer, K., Venas, M. and Hopperstad, O. S. (2019). A thermo-elasto-viscoplastic constitutive model for polymers: Formulation and numerical implementation. Polym. Test., 74, pp. 14–26. DOI: https://doi.org/10.1016/j.polymertesting.2019.02.017.
[32] Aour, B., Zaïri, F., Gloaguen, J. M., Naït-Abdelaziz, M. and Lefebvre, J. M. (2008). A computational study of die geometry and processing. Int. J. Mech. Sci. 50(3), pp. 589-602. DOI: https://doi.org/10.1016/j.ijmecsci.2007.07.012.
[33] Yamaguchi, D., Horita, Z., Nemoto, M. and Langdon, T. G. (1999). Significance of adiabatic heating in equal-channel angular pressing. Scr. Mater., 41(7), pp. 791–796. DOI: https://doi.org/10.1016/S1359-6462(99)00233-X.
[34] Aour, B., Zaïri, F., Gloaguen, J. M., Naït-Abdelaziz, M. and Lefebvre, J. M. (2006). Numerical investigation on equal channel angular extrusion process of polymers. Comput. Mater. Sci., 37(4), pp. 491–506. DOI: https://doi.org/10.1016/j.commatsci.2005.11.008.
[35] Beyerlein, I. J. and Tomé, C. N. (2004). Analytical modeling of material flow in equal channel angular extrusion (ECAE). Mater. Sci. Eng.: A, 380(1–2), pp. 171–190. DOI: https://doi.org/10.1016/j.msea.2004.03.063.